"POLITEHNICA" UNIVERSITY OF BUCHAREST

Doctoral School of Electronics, Telecommunications and Information Technology

Decision no 964 from 16.11.2022

THESIS

-SUMMARY -

Ing. Mircea NICOLAESCU

CONTRIBUȚII PRIVIND COMPATIBILITATEA ELECTROMAGNETICĂ A CIRCUITELOR ȘI SISTEMELOR DIGITALE

CONTRIBUTIONS REGARDING ELECTROMAGNETIC COMPATIBILITY OF DIGITAL CIRCUITS AND SYSTEMS

THESIS COMMITTEE

Prof. Dr. Eng. Ion MARGHESCU "Politehnica" University of Bucharest	President
Prof. Dr. Eng. Victor CROITORU "Politehnica" University of Bucharest	PhD supervisor
Prof. Dr. Eng. Dumitru Nicolae ALEXANDRU "Gheorghe Asachi" Technical University of Iași	Reviewer
Prof. Dr. Eng. Gavril TODEREAN Technical University of Cluj-Napoca	Reviewer
Prof. Dr. Eng. Norocel Dragoș CODREANU "Politehnica" University of Bucharest	Reviewer

BUCHAREST 2022

Content

1. Introduction

The evolution of the human society from the industrial era to the information age has produced major changes towards the connectivity between people and human groups, towards the speed of transmission, as well as the information content. Large scale integration techniques, system on a chip, FPGA-urile etc. led to scale down the electronic devices, low power consumption and increased operational speed. The study published by IEEE International Roadmap for Devices and Systems (IRDS-2020) [1] points out the main semiconductor based industries which experience high growth rates: Deep learning, high performances data centers, high speed radio an fiber optic nets, IoT-uri, remote medical systems, vehicular industry, smart houses/cities, entrainment industry etc.

All the above mentioned applications use digital systems that are integrated into high complexity systems, which provide high processing and transmission speed of data and information [2] and that operate in highly crowded electromagnetic medium. As a result, the risk of these systems disrupting or being disrupted by other applications is high

1.1 Presentation of the doctoral domain

The following theological tendencies are present in the field of digital circuits and systems: increasing the complexity of the integrated circuits, decreasing the power and increasing the operating frequency and the transfer rate of the I/O devices. All of these lead to an increased probability of mutual perturbation of the systems that work in an limited area. Therefore the electromagnetic compatibility analysis in the design stage is a necessity. The electromagnetic compatibility studies the needed conditions such as electrical, electronic, communications, IT, command and control equipment used in industrial, medical, research, surveillance and domestic applications, to acquire, process, store and transfer information generate no interferences and are not affected by neighboring systems, in a medium with specified electromagnetic parameters.

Nowadays the measurements in the field of integrated circuits are carried out till 6 GHz, and the standards as IEC 61967 [12] for emission and IEC 62132 [13] [14] for immunity cover the bandwidth 150 kHz -1 GHz. There are proposals till 3-6 GHz, and 10-25 GHz respectively, such as GTEM (GHz – Transverse Electromagnetic Mode) cells. On the other hand the 5G generation devices work in the bands 24,25-27,5 GHz and 26,5 – 29,5 GHz, and 6 G can reach 100-200 GHz. This means that the current standards has to be updated in order to over the above mentioned frequency ranges [2].

1.2 The goals of the doctoral thesis

The electromagnetic compatibility is a high complexity area, whose importance increased in the last years due to the fast development of different types of electronic circuits, due to the miniaturization and the growth of the integration level and of the frequency. The information and command control signals sent between different parts of a digital system are trapezoidal pulses. The goals of the doctoral thesis are directed to the analysis of some aspects with regard to electromagnetic compatibility of digital circuits and systems, as follows:

- The analysis of the bandwidth of the trapezoidal pulses used to send information as well as for command/control signals within digital circuits and systems.
- The modelling of some microstrip connections in order to analyze the dependency of the reflection, transmission and coupling parameters on the lines separation at high frequency.
- The evaluation by simulation of the reflection, transmission and coupling parameters for a differential pair in time and frequency domains.
- The evaluation of the radiated power and radiated electric fields by via and vias and microstrip lines, as a function of frequency (1-40 GHz).
- The study of the variation of the electromagnetic field as a function of angles and frequency for vias and microstrip lines.
- Performing the simulation and evaluate the radiated power and radiated electric fields as a function of frequency (1-40 GHz) by a slot.
- The modelling of a radiation source within an desktop enclosure and evaluate the electric field transmitted outside the enclosure.
- Performing some experiments based on simulated cases.

1.3 The content of the doctoral thesis

The PhD thesis has 8 chapter and a section with references. The subject and state of the art in the field of electromagnetic compatibility are presented in the introduction. Likewise, the main objectives are listed and a short description of each chapter is presented.

Chapter 2, Spectral characterization of the digital signals, is for spectral analysis of signals transmitted within digital circuits and systems. Periodic trapezoidal pulses are analyzed in frequency and time domains in order to determine the maximum frequency that has to be used for electromagnetic compability pursposes.

In the next chapter, The study of the coupling between the connections among circuits and digital systems using the electromagnetic field method, the microstrip lines are analyzed from the perspective of interference signals that are transmitted from an active line to a passive line arranged at a certain distance. The analyzed lines are made on Rogers 4003 C substrate which has low losses in the analyzed frequency band. The maximum frequency set in the previous chapter is 50 GHz.

Chapter 4, Analysis of microstrip lines fed with differential signals manufactured on Rogers 4003 C microwave substrate, presents the main theoretical aspects of differential lines and studies the coupling between the two lines in the case of a differential pair. The analysis of the differential pair is performed in the case of common mode signal and differential signal feeding.

A large part of the connections made between different digital circuits consist of vias and microstrip line segments. Currents flowing through these connections will cause electromagnetic interferences. In Chapter 5, Determination of radiated field by vias and microstrip lines in digital circuits and systems, the radiation properties of these elements are analyzed.

Chapter 6, The study of the field radiated through a slot in the ground plane and in the case of a desktop computer, is intended to study the electromagnetic interferences

transmitted by radiation by slots cut in the ground plane or in the case of a desktop computer. In order to determine the radiated electromagnetic field, the distribution of the electromagnetic field on the radiant surface is calculated.

Chapter 7, Experimental results, is intended to present the experimental results obtained. In order to analyze the coupling between 2 and 3 microstrip lines, several PCBs with 3, 4 and 5 microstrip lines arranged at different distances, with and without a slot in the ground plane, were manufactured. PCBs were made on a Rogers 4003 C substrate due to lower losses at high frequencies compared to FR4. The measurements were performed in the band 1-40 GHz, with a vector netork analyzer, and the results were compared with those obtained by simulations. Other measurements were performed to determine the radiated field by a via connected to an open microstrip line or terminated on matched load. The last part of this chapter describes the measurement configurations and the results obtained for determining the radiated field by a slot made in the case of a desktop computer. Chapter 8 is devoted to the conclusions and original contributions.

2. Spectral characterization of the digital signals

The analysis of the effects of the communication channel on the transmitted signals can be performed in the time domain, by varying the time parameters such as: duration, repetition period, front times and amplitude, and in the frequency domain by applying the Fourier series [18] [19] and spectrum determination (frequency and amplitude of the spectral components). The analysis of digital signals in the frequency domain allows the definition of the working band and the identification of some causes that lead to the degradation of the signal in the link channel. Therefore, in this chapter the spectral composition of rectangular and trapezoidal digital signals is studied.

Analysis of rectangular signals in the frequency domain

The transmission of information-carrying and control signals without distortion requires knowledge of their band. This is determined by applying the Fourier series to the analyzed signal. Note the time signal with u (t). It can be written as an infinite sum of sinusoidal signals [21]:

$$\dot{u}(t) = \sum_{n=-\infty}^{\infty} c_n e^{jn\omega_0 t} \tag{2.1}$$

where: - $\dot{u}(t)$ is the complex signal, c_0-amplitude of the direct current component (DC) and c_n-amplitude of the spectral component with frequency $nf_0=n/T$.

After performing the calculations, the expression of the signal u (t) becomes:

$$\dot{u}(t) = U\frac{t_i}{T} + 2U\frac{t_i}{T}\sum_{n=1}^{\infty}\left[\frac{\sin\left(n\pi f_0 t_i\right)}{n\pi f_0 t_i}\right] e^{-j\pi n f_0 t_i} e^{j2\pi n f_0 t}, \tag{2.5}$$

For frequencies between 0 and $1/\pi t_i$ the amplitude of the spectral components is constant, while the amplitude of the spectral components with a frequency higher than $1/\pi t_i$ decreases by -20 dB per decade.

Analysis of trapezoidal signals in the frequency domain

Like any periodic signal, the trapezoidal pulse can be written as an infinite sum of sinusoidal signals having frequencies equal to multiples of the fundamental frequency. The determination of the spectral composition of a series of trapezoidal pulses is performed by applying the Fourier series. The following expression is obtained for the complex signal:

$$\dot{u}(t) = U\frac{t_i}{T} + 2U\frac{t_i}{T}\sum_{n=1}^{\infty}\left[\frac{\sin\left(n\pi f_0 t_i\right)}{n\pi f_0 t_i}\right]\left[\frac{\sin\left(n\pi f_0 t_f\right)}{n\pi f_0 t_f}\right]e^{-j\pi n f_0(t_i+t_f)}e^{j2\pi n f_0 t}. \quad (2.12)$$

The trapezoidal pulse described by the function u(t), assuming that the front times are equal, has a direct current component Ut_i/T and an infinity of harmonics with the amplitude:

$$2U\frac{t_i}{T}\sum_{n=1}^{\infty}\left[\frac{\sin\left(n\pi f_0 t_i\right)}{n\pi f_0 t_i}\right]\left[\frac{\sin\left(n\pi f_0 t_f\right)}{n\pi f_0 t_f}\right]. \quad (2.14)$$

Since 2 functions of the form sin (x)/x appear, it results that the graph has 2 inflection points, in which the slope varies by -20 dB per decade. The two inflection points are given by the pulse duration and the front time. In the more general case, when the rising and falling front times are different, 3 inflection points will appear, corresponding to the duration and times of the front. The position of the second inflection point depends on the front time. The trapezoidal pulses were considered to be symmetrical, therefore the durations of the two fronts are equal. Some authors consider that the band of a periodic trapezoidal signal is given by this inflection point [21]. There are also authors [22] who, from the perspective of electromagnetic compatibility, consider the band to be given by $1/t_f$.

Determination of the maximum frequency of the harmonic useful in signal recovery

The band of a digital signal is determined by the spectral component with the maximum frequency, which is relevant in signal recovery. The weight of a spectral component in the recovery of the digital signal can be determined on the basis of the power budget or on the basis of the deviation of the recovered signal, by summing up a finite number of spectral components, compared to the real shape.

The signal in the time domain with a frequency of f_0=5 GHz, a value encountered in computing systems, and the fill factor, t_i/T, equal to ½, was decomposed, using the Fourier series, into 100 cosinusoidal signals. The determination of the spectral component with maximum frequency that has a significant weight in signal recovery is performed by comparing the signal obtained by summing the continuous component and the first N harmonics with a reference signal obtained by summing the continuous component and the first 100 harmonics.

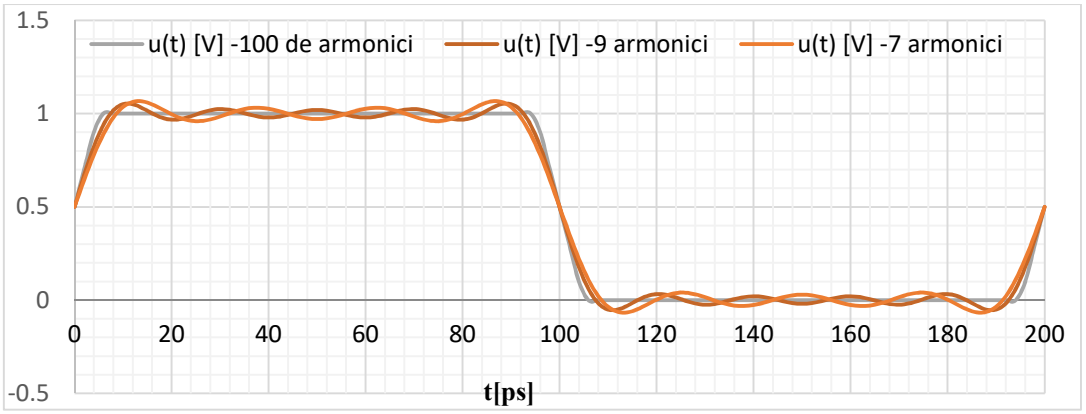

Figure 2.11 Periodic trapezoidal pulse with t_i = 100ps, T = 200ps and t_f = 10ps, redone with the first 100 harmonics (reference), with the first 7 and 9 harmonics, respectively.

The restored trapezoidal pulse with the value of direct current and the first 7, respectively 9 spectral components is represented on figure 2.11. The maximum amplitude variation is 6.53% for the case with 7 harmonics, respectively 5% for the first 9 harmonics. Front time increases to 16 ps for 7 harmonics and to 14 ps for 9 harmonics.

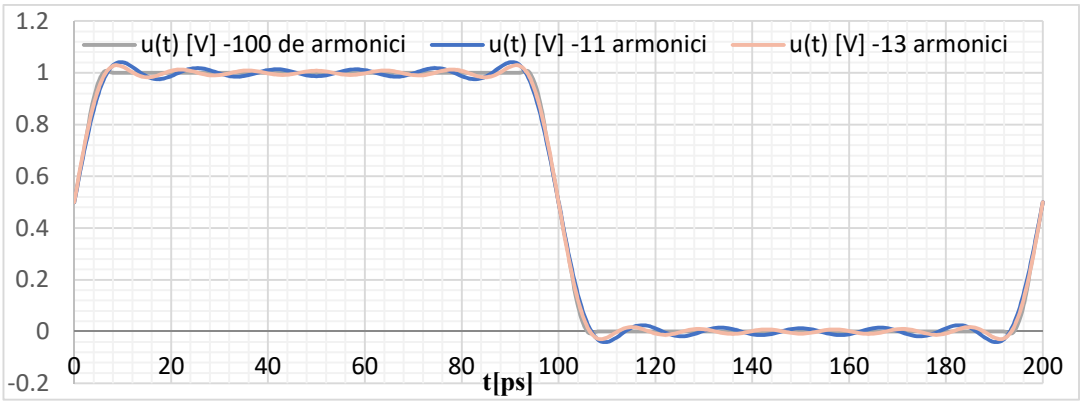

Figure 2.12 Periodic trapezoidal pulse with t_i = 100ps, T = 200ps and t_f = 10ps, redone with the first 100 harmonics (reference), with the first 11 and 13harmonics, respectively.

The use of more spectral components reduces the ripple on the pulse level to 4% for 11 harmonics and to 2.66% for 13 harmonics, respectively, as can be seen in figure 2.12. In this case the front times are approximately equal.

Using the approximate bandwidth ratio of $0{,}435/t_f$ results a maximum frequency of 43.5 GHz, while the use of the first 9 harmonics means a maximum frequency of 45 GHz, respectively for 11 harmonics 55 GHz.

Determination of the spectral composition of digital pulses by simulations

The simulations were performed using different pulse parameters established based on the working frequencies of some electronic equipment. In order to make some comparisons, simulations were performed for periodic rectangular and trapezoidal pulses (U_i=1V, t_i=100 ps, T=200 ps și t_f=10 ps).

By applying the Fourier series to the signal with the parameters mentioned above, the spectral components shown in figure 2.20 are obtained, in the range 0-50 GHz.

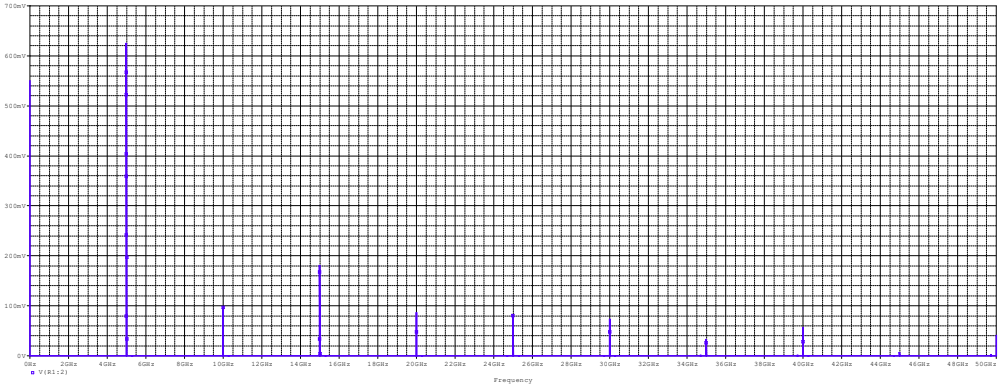

Figure 2.20 Spectrum of trapezoidal pulses with the parameters:U_i=1V, t_i=100 ps, T=200 ps și t_f=10 ps

The spectrum shown in Figure 2.20 contains both even and odd harmonics. The spectral component with a frequency of 40 GHz has an amplitude of 60 mV (6% of the maximum signal amplitude) and the one with 50 GHz an amplitude of 40 mV (4% of the maximum signal amplitude). The result is:

$$Banda = \frac{0,4375}{t_f} = \frac{0,4375}{10 \cdot 10^{-12}} Hz = 43,75 \quad GHz \cdot \tag{2.25}$$

Conclusions

In this chapter, different variants of rectangular and trapezoidal pulses in the frequency domain were analyzed, in order to determine the maximum frequency harmonic to be taken into account in the electromagnetic compatibility analyses. The determination of the spectral components was performed by analytical calculation and by simulations. The results obtained indicate the weight of the number of harmonics on the signal ripple and on the front times. The simulations showed that for n> 5, the use of a larger number of harmonics has a greater influence on the improvement of the front time than on the variation of the amplitude. Given the working frequencies of electronic equipment and its increasing trend, it turns out that the maximum frequency in the working band is in the range of 40-50 GHz.

The main contributions in this chapter relate to:

- Theoretical analysis of the band of a trapezoidal pulse and comparison of the relations presented in the literature according to which the maximum frequency is given by $1/\pi t_f$, respectively $1/t_f$, resulting that the relation that provides the closest results to those obtained by simulations is $0.609 /t_f$.
- Determining the spectral components of some rectangular pulses, restoring the signal with a limited number of harmonics and analyzing the influence of the number of spectral components used in restoring the signal on the amplitude of the pulses and on the front times.
- Performing PSpice simulations to determine the spectral components and establishing the theoretical relationship that provides the best approximation of the relevant maximum frequency in terms of electromagnetic compatibility.

3. The study of the coupling between the connections among circuits and digital systems using the electromagnetic field method

3.1 Introduction

Disturbing signals that reach a digital system or a device by coupling come from several sources, which are considered independent. Therefore, the evaluation of the coupling must be performed using the superposition (the effects produced by independent sources are cumulated in the case of linear, passive systems) [21].

3.2 Coupling in digital systems

The characterization of the coupling between two or more circuits can be performed using circuit methods or methods based on electromagnetic field calculation. In the first case, an equivalent circuit of the two coupled lines is developed. The models used for the lines must take into account the geometric structure, the input and load impedances and allow the calculation of the voltages. A widely used model involves the approximation of coupled lines with n sections of circuit with concentrated constants, the coupling being described by mutual capacitances and inductances [25] [31].

Consider two coupled lines, terminated on 50 ohm impedances, as in Figure 3.3. It is denoted by C_m, L_m coupling capacity and inductance, respectively C_{mul}- mutual capacitance per unit length, L_{mul}- mutual inductance per unit length, R_{ul}-resistance per unit length, G_{ul}-conductance per unit length, L_{ul}-inductance per unit length and C_{ul}-capacity per unit length.

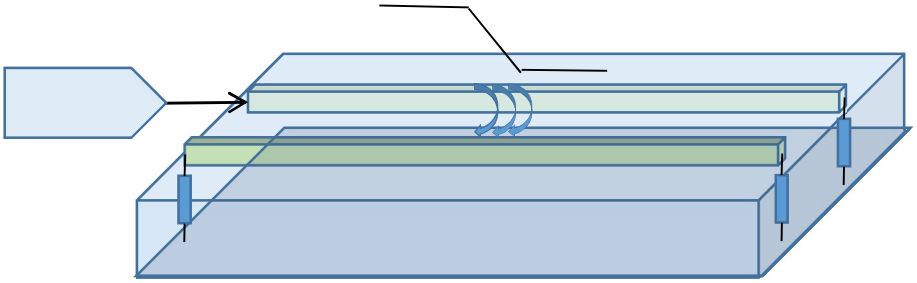

Figure 3.3 The region in which the signal is transmitted from the active line to the passive line is where the voltage and current vary [11].

The total current flowing through coupling capacitors is [25]:

$$I_C = C_m \frac{dU}{dt} \tag{3.2}$$

I_C- the noise current transmitted through capacitive coupling;
t_{fc}- defined duration of 10-90% of the rising front.

$$C_m = C_{mul} \times \Delta x = C_{mul} \times v \times t_{fc} \tag{3.3}$$

The capacitive coupling current I_c

$$I_C = C_{mul} \times v \times t_{fc} \times \frac{U}{t_{fc}} = C_{mul} \times v \times U \tag{3.4}$$

v- the signal propagation speed ($c/\sqrt{\varepsilon_{ref}}$); Δx - lungimea celulei; c- is the speed of light in vaccum-3 10^8 m/s; ε_{ref} – the relative dielectric permittivity.
Inductive coupling voltage is:

$$U_L = L_m \frac{dI}{dt} = L_{mul} \times v \times t_{fc} \times \frac{I}{t_{fc}} = L_{mul} \times v \times I \tag{3.5}$$

U_L – Inductive coupling voltage.

The duration of the pulse induced at the near end will be $2xt_{int}$. If the pulse rise time applied to the active line is equal to $2xt_{int}$, then the pulse induced at the near end reaches its maximum value, after which it begins to decrease. The saturation length (l_{sat}) is [25]:

$$l_{sat} = \frac{1}{2} \times t_{int} \times \frac{c}{\sqrt{\varepsilon_{ref}}} \quad . \tag{3.6}$$

3.3 Distribution parameters (S)

A device with two ports can be characterized by several parameters: H, Y, Z; based on voltages and currents at the two ports (measurable quantities at low frequency) [27]. At very high frequencies a short circuit behaves like a inductance and a gap like a parasitic capacitance. It turns out that other parameters are needed to characterize high frequency devices. These are called the distribution parameters and are defined as function of the incident, reflected and transmitted waves.

3.4. Coupling analysis using electromagnetic field simulations

Since the analysis performed on FR4 in the papers presented at Comm 2020 [43] [44] shows that the losses in this substrate are high at frequencies higher than 10 GHz, Rogers 4003 C was chosen as a microwave substrate, which has reasonable properties at relatively low costs and a dielectric permittivity of 3.55.

In order to perform the simulations for the study of microstrip lines, a model was built in the simulation program with the following parameters: lL -the length of the microstrip line-6 cm; lw -the width of the microstrip line -3.1 mm; sh - the substrate thickness-1.524; ch - the conductor thickness -0.035mm; sL- the substrate length - 6 cm; sl- the substrate width -6 cm; ld- the line separation- 1.1; 3.1; 5.1; 7.1; 9.1 mm.

The simulations were performed in a high band, 0.5-50 GHz (with a step of 0.1 and 0.5 GHz), taking into account the maximum working frequency reached as well as the growth prospects in the near future [34]. In order to feed the two transmission lines, the terminal type ports were used to which 1 V voltages were applied. To determine the radiated waves, the chosen power level was 1mW, the default level being 1 W. A lower power than the default was chosen considering the experimental part, the laboratory

generators ensuring a maximum level of 10 mW. The simulations were carried out using a 50 ohms impedance as reference, so the modulus of S_{33} parameter in dB is:

$$S_{33}\left[dB\right] = 20\log\left|\frac{Z_{in}-50}{Z_{in}+50}\right|. \tag{3.82}$$

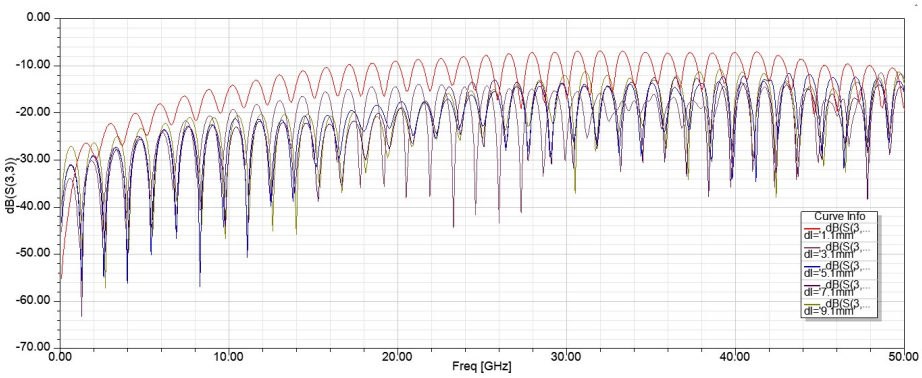

Figure 3.13 The variation of the reflection parameter S33, as a function of frequency, for two microstrip lines with different separations: 1.1; 3.1; 5.1; 7.1 and 9.1 mm.

On Figure 3.13 one can see that the separation between the two lines affects the value of the reflection parameter S_{33}. It reaches a maximum value of -8 dB, for dl=1.1 mm. If the separation between the microstrip lines is increased to 3.1 mm and then to 5.1 mm; 7.1 mm and 9.1 mm the influence of the crosstalk against the input impedance of port 3 is much lower. On the same time, it can be noticed that the values of S_{33} for dl=5.1mm; 7.1 mm and 9.1 mm are comparable.

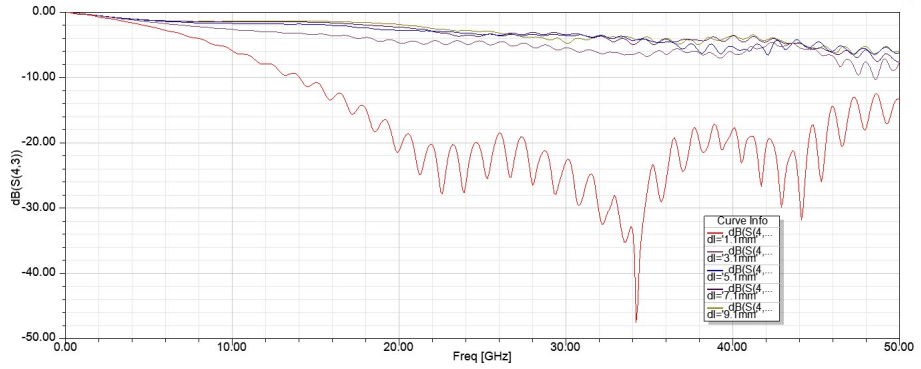

Figure 3.14 The variation of the transmission parameter S_{43}, as a function of frequency, for two microstrip lines with different separations: 1.1; 3.1; 5.1; 7.1 and 9.1 mm.

The transmission parameter, S_{43}, represented on Figure 3.14, describes the ratio between the voltages obtained at port 4 and port 3 as a function of the separation between the lines. A frequency variable, from 0.5 GHz to 50 GHz, 1 V voltage is applied at port 3.

$$S_{43}\left[dB\right] = 20\log\left|\frac{U_{ies4}}{U_{in3}}\right| \tag{3.83}$$

The transmission parameter depends on the separation between the traces. If the two lines are around one third of the line width apart (1.1 mm) then S_{43} is strongly influenced by the passive line. It decreases till -20 dB when frequency changes from 0.5 GHz to 20 GHz, while, for frequencies between 20 GHz and 45 GHz, the values of S_{43} varies in the

range of -20 dB to -30 dB, and then they rise to -15 dB. When the separation is the same as the width of the microstrip line (3.1 mm), the attenuation increases proportionally with the frequency, reaching the maximum value of -10 dB at 50 GHz. For the other separations the curves describing the attenuation are similar, reaching a maximum value of -8 dB at 50 GHz.

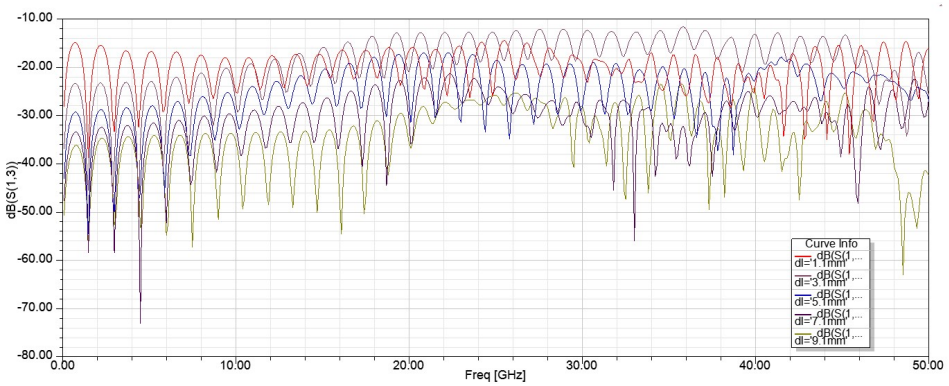

Figure 3.15 The variation of the coupling parameter S_{13}, as a function of frequency, for two microstrip lines with different separations: 1.1; 3.1; 5.1; 7.1 and 9.1 mm.

The near end coupling (Figure 3.15) signal varies, in average, between -40 dB and -20 dB, depending on the distance between the two traces and the maximum values are reached in the frequency range - 20-30 GHz and the curves for 7.1 and 9.1 mm separations are very similar in shapes and the values are quite close each other. In the frequency band 18-44 GHz the near end coupling signal is higher for 3.1 mm separation, against 1.1 mm separation.

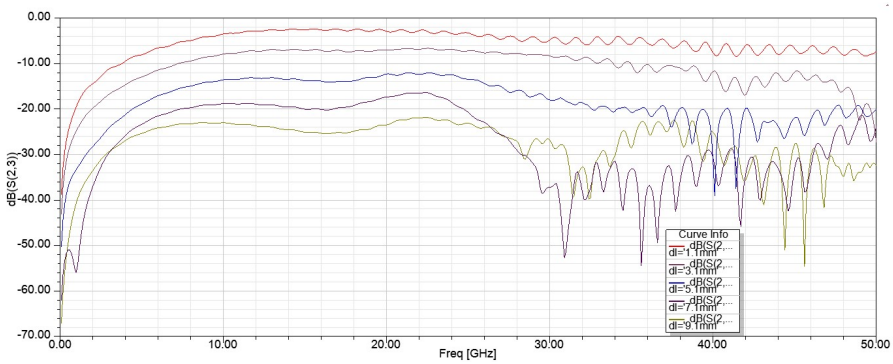

Figure 3.16 The variation of the coupling parameter S_{23}, as a function of frequency, for two microstrip lines with different separations: 1.1; 3.1; 5.1; 7.1 and 9.1 mm.

With regard to the coupling signal at the far end, port 2, Figure 3.16 shows a decrease of the coupling as separation increases from 1.1 mm to 3.1 mm and to 5.1 mm. The maximum value of the coupling signal for a separation of 1.1 mm is reached in the frequency range 10-20 GHz, then it diminishes.

3.5 Conclusions

This chapter presents some of the electromagnetic compatibility issues raised by the coupling between connections among circuits with digital systems. After a theoretical presentation of some aspects related to the modeling of the coupling, the capacitive and the inductive coupling, as well as the determination of the voltages at both ends of a coupled line, the distribution parameters are used, used to characterize very high

frequency circuits. In the chapter the coupling is analyzed using the electromagnetic field method.

The simulations and practical determinations were performed on a Rogers 4003 C substrate, which is reasonably priced and covers the 1-50 GHz band.

Own contributions in this chapter relate to:

- Modeling of two single lines made on a low loss Rogers 4003 C substrate for high speed PCBs;
- Study with the electromagnetic field method of the variation of the parameters of two coupled lines;
- Analysis of reflection and transmission parameters in the 1-50 GHz band, depending on the distance between the lines (1.1; 3.1; 5.1; 7.1 and 9.1 mm);
- Study of the variation of the coupling parameters at the near and far ends in the band 1-50 GHz, depending on the distance between the lines (1.1; 3.1; 5.1; 7.1 and 9.1 mm).

4. Analysis of microstrip lines fed with differential signals manufactured on Rogers 4003 C microwave substrate

4.1 Introduction

A differential pair consists of two transmission lines that have a certain level of coupling between them. This configuration is used due to the advantages of differential signal transmission. It involves the use of two transmission lines fed by two complementary signals, the information being contained in the difference signal. Among the advantages offered by the use of differential signals we can mention the robustness to external disturbances, the generation of smaller interference signals due to the smaller variations of the control currents and the possibility of using differential amplifiers, which have a higher gain than the ones asymmetrically fed.

However, if the differential signals are not perfectly synchronized and common mode components appear, they will generate electromagnetic interferences. Another disadvantage is that the transmission of differential signals requires a double number of conductors. Differential signals are widely used in computing system interface (SCSI) buses, in Ethernet, in many high-power optical communication protocols, OC-48, OC-192, 768, and in all high-speed systems. One of the most used schemes is LVDS (Low Voltage Differential Signaling) [25].

The impedance seen by the differential signal represents the ratio between the voltage and the current between the two lines. When differential feeding, one line is connected to + U_{sing}, and the other to -U_{sing}. The differential voltage is 2 U_{sing}, which gives:

$$Z_{dif} = \frac{U_{dif}}{I_{sing}} = \frac{2 \times U_{sing}}{I_{sing}} = 2 \times \frac{U_{sing}}{I_{sing}} = 2 \times Z_0, \quad (4.5)$$

where: I_{sing} – the current on a single ended line; U_{sing} – the voltage between the signals trace and return path in a single ended line; Z_0 – the characteristic impedance of a single ended line; Z_{dif} - the differential impedance.

Consider two microstrip lines fed by U_1, U_2. The differential pair can be fed in two ways, in phase and out of phase. If a differential line is fed in one of two modes, the signal propagates undistorted and the modes are called even and odd. Modes are intrinsic properties of the differential line and are used to define different feeding schemes.

The terms common and differential describe the command signals. The differential part is given by the difference between the two signals, while the common part represents the average of the signals. The differential signal propagates in the odd mode, while the common signal propagates in the even mode. The terms even and odd can be used to describe any signal.

Differential (mixed) S parameters describe the interaction of differential and common signals with the connections.

4.2 Study of the differential pair with the electromagnetic field method

For the differential feeding of the two microstrip lines, two "wave" type ports were created at the two ends of the structure, the two lines being defined as differential pair. They are fed in odd mode, with complementary voltages (with the same amplitude, but out of phase by 180 degrees), respectively in even mode with identical voltages. The chosen power level was 1 mW.

Analysis of reflection parameters

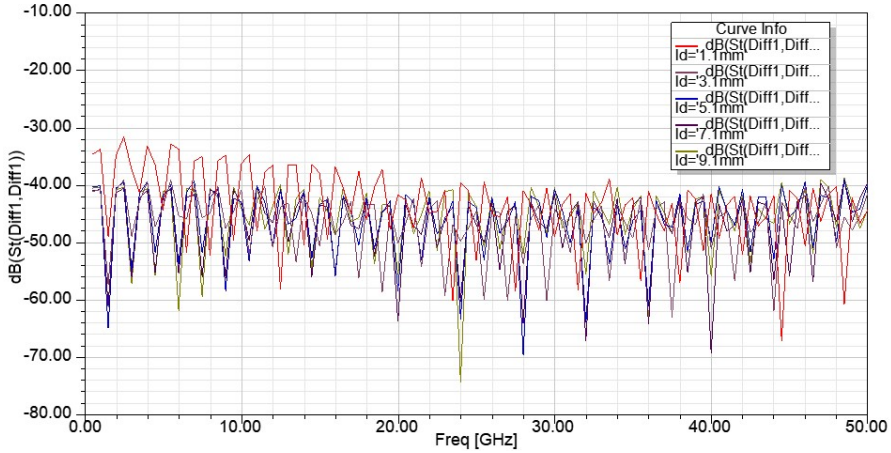

Figure 4.7 Variation of the reflection parameter St (diff1, diff1), depending on the frequency, in the case of two microstrip lines with a width of 3.1 mm for different distances between lines (1.1; 3.1; 5.1; 7; 7 , 1; 9.1 mm).

The parameter St(diff1,diff1) indicates the ratio between the differential voltage reflected at port 1 against the input differential voltage. The diagrams presented in Figure 4.7 show that for ld= 3.1; 5.1; 7.1; 9.1 mm the values of the reflection coefficient are less than -40 dB, and the shapes of the curves are quite similar. For a distance of 1.1 mm,

the reflections are higher, in average with 5 dB from 0,5 to 20 GHz, and for the entire frequency range the shape is different.

For a distance greater than or equal to 3.1 mm the level of the reflected signal is about – 40 dB, and the distance dependence between the lines is very weak.

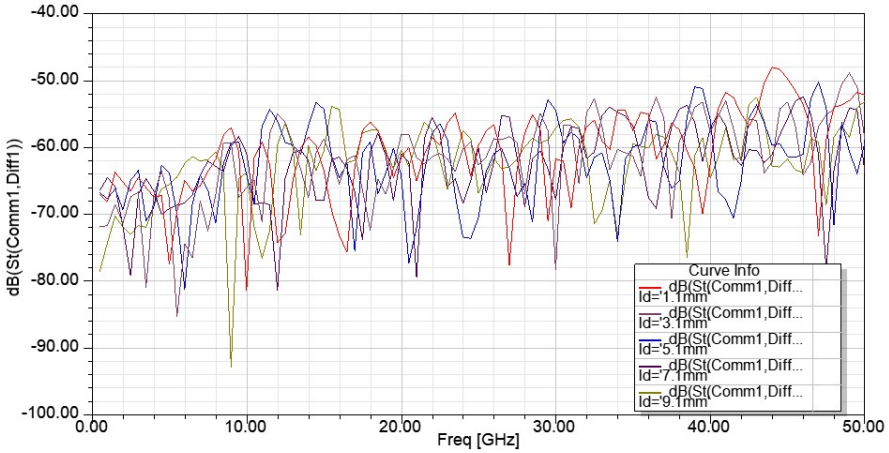

Figure 4.8 Variation of the reflection parameter St (comm1, diff1), depending on the frequency, in the case of two microstrip lines with a width of 3.1 mm for different distances between lines (1.1; 3.1; 5.1; 7; 7 , 1; 9.1 mm).

In the case of the differential feeding of a pair of microstrip lines, a common mode component also appears, due to the return currents flowing through the ground plane. From the performed simulations, presented in figure 4.8, it is found a reduced dependence of the parameter St (comm1, diff1) on the distance between the lines. It increases with frequency, reaching about -50 dB at maximum frequency. As a result, in the case of differential feeding, there is a difference of at least 10 dB between the differential mode and the common mode component.

Analysis of transmission parameters

When a differential signal is applied to the input of the microstrip pair, the common mode signal that appers propagates to port 2. The parameter by which the level of the transmitted common mode signal is measured is St (comm2, diff1).

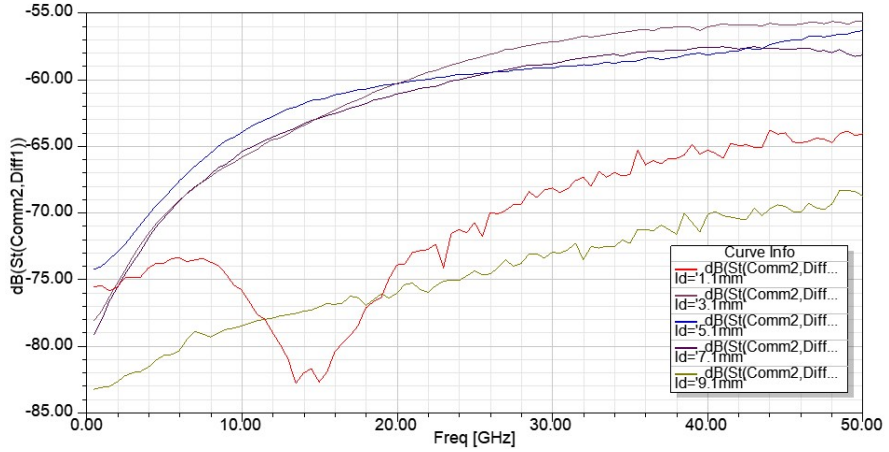

Figure 4.9 Variation of the transmission parameter St (comm2, diff1), depending on the frequency, in the case of two microstrip lines with a width of 3.1 mm for different distances between lines (1.1; 3.1; 5.1; 7; 7 , 1; 9.1 mm).

On Figure 4.9 can be seen that for separations of 3.1, 5.1 and 7.1 mm the shape of the curve are the same, with some variations within the range of 6 dB and the maximum

value of -54 dB. For a separation between the lines of 1.1 mm the common signal ranges between -75 dB and -65 dB, values smaller with around 10 dB for frequencies higher than 10 GHz.

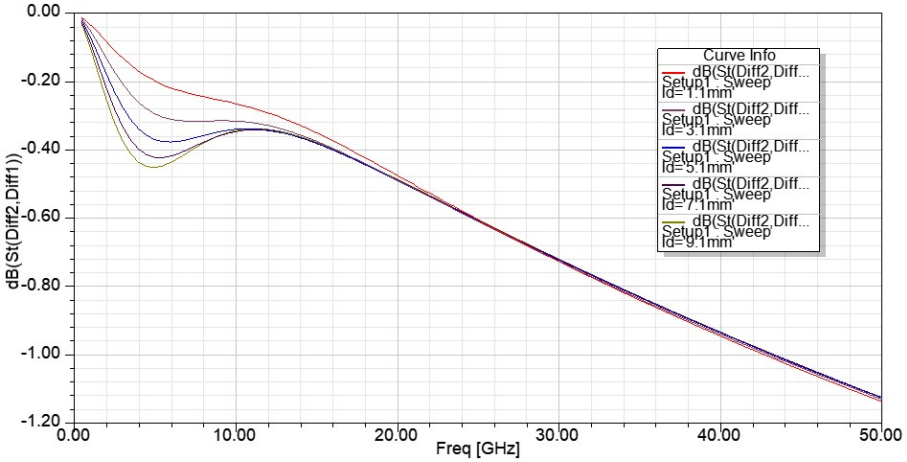

Figure 4.10 Variation of the transmission parameter St (diff2, diff1), depending on the frequency, in the case of two microstrip lines with a width of 3.1 mm for different distances between the lines (1.1; 3.1; 5.1; 7; 7 , 1; 9.1 mm).

The parameter St (diff2, diff1), represented in figure 4.10, indicates the losses of the differential signal when covering the distance of 60 mm. Propagation losses are influenced by the distance between the two microstrip lines up to a frequency of 15 GHz. At frequencies above this value the respective curves overlap. Losses also increase as the distance between the microstrip traces increases. Curves describing losses have a local minimum around 5 GHz.

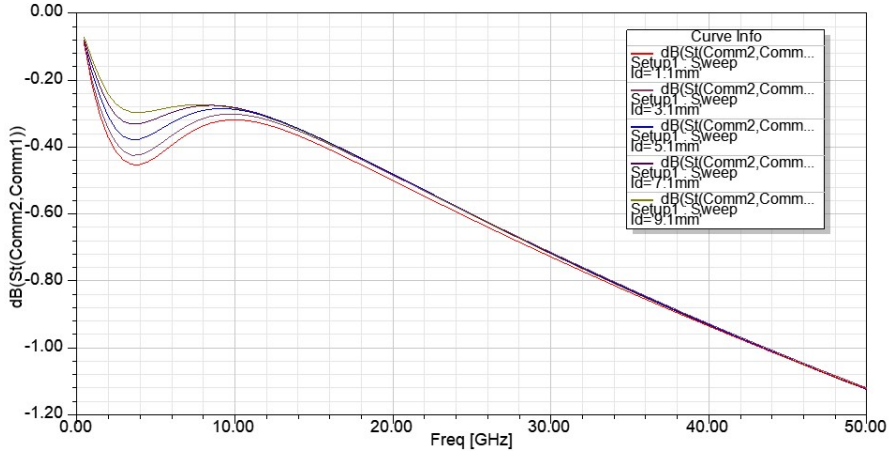

Figure 4.11 Variation of the transmission parameter St (comm2, comm1), depending on the frequency, in the case of two microstrip lines with a width of 3.1 mm for different distances between lines (1,1; 3,1; 5,1; 7 , 1; 9.1 mm).

The parameter St (comm2, comm1) in figure 4.11 indicates the attenuation of the common signal. The simulations show a similar variation for the 5 distances between the lines, but the curves are arranged in reverse order to the previous case, respectively the maximum attenuations are obtained if the distance between the lines is 1.1 mm.

Determination of the differential impedance

The differential impedance represents the impedance of the two lines when two signals with equal amplitudes are applied to their inputs, but out of phase by 180 degrees (+1 V and -1 V). If the two lines were independent, i.e there was no coupling between

them, the impedance in the case of differential feeding is twice the input impedance of a single line.

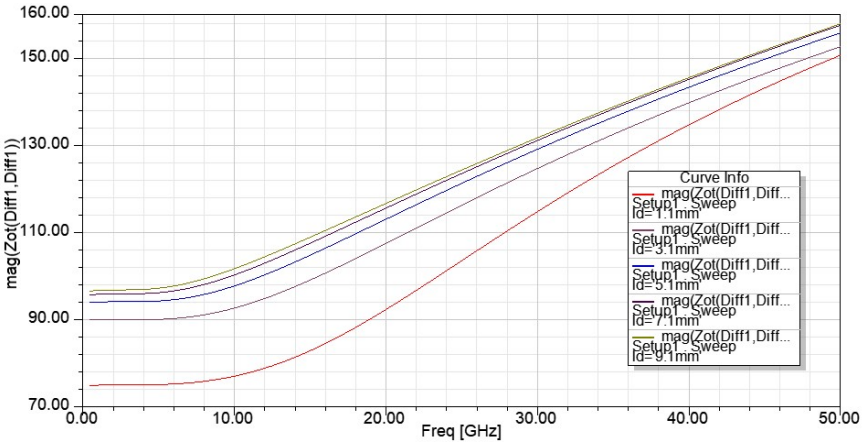

Figure 4.12 Impedance variation Z0t (diff1, diff1), depending on the frequency, in the case of two microstrip lines with a width of 3.1 mm for different distances between the lines (1.1; 3.1; 5.1; 7, 1 9.1 mm).

The graphs in Figure 4.12 show that the impedance is approximately constant up to about 10 GHz, after which it increases proportionally to the frequency, with different growth rates depending on the distance between the two microstrip lines. The simulations performed for different values of the distance between the lines indicate that for a separation of about 1/3 of the line width there is a very tight coupling between the two lines that influences the value of the differential impedance. The coupling decreases with increasing distance.

4.3 Analysis of the differential pair in the time domain

In order to analyze the operation of the differential pair in transient mode, the S parameters determined at the frequency of 10 GHz, were saved in a Touchstone file, then a Circuit Design project was launched. Two pulse sources were used to feed the differential pair: U_1 = 1 V and U_2 = -1 V, pulse duration t_i, rising edge t_{fc}, decreasing front t_{fd}, delay-t_{intar}.

In order to analyze the transient regime, the equivalent circuit was imported into PSpice in the form of a user-created block, then the differential feeding scheme was made (t_i=280 ps, t_{fc} =20 ps, t_{fd} =20 ps, t_{intar}=10ps).

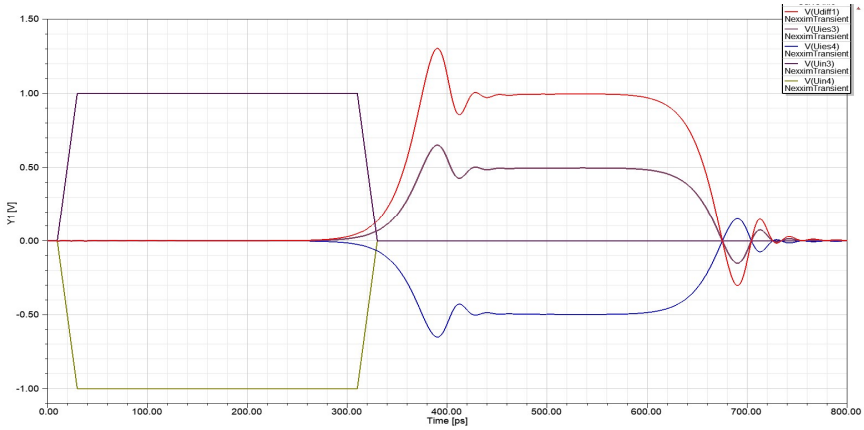

Figure 4.21 Variation of voltages at the input and output of the two microstrip lines fed differentially with trapezoidal pulses lasting 280 ps and fronts 20 ps.

Figure 4.21 shows an increase in the amplitude of the oscillations produced by the passage through the differential line to about 40%.

For a 5 GHz clock frequency, a pulse repetition period of 100 ps and a front time of 10 ps are used (Figure 4.22 -t_i=100 ps, t_{fc} =10 ps, t_{fd} =10 ps, t_{intar}=10ps).

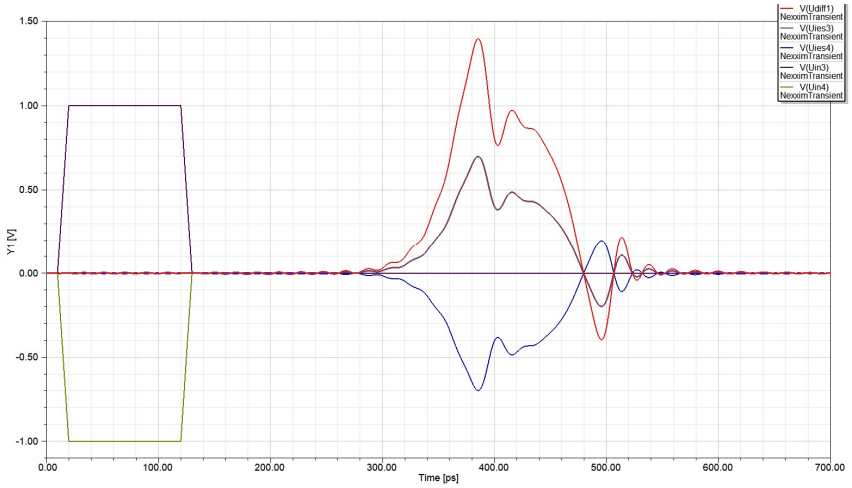

Figure 4.22 Variation of voltages at the input and output of the two microstrip lines fed differentially with trapezoidal pulses lasting 100 ps and fronts 10 ps.

Figure 4.22 shows that in this case the pulse obtained at the output of the differential line is deformed, and the maximum amplitude of the oscillations reaches 60% of the amplitude of the pulse applied at the input.

Other problems that cause interferences in the case of a differential pair are given by the differences in propagation times between the two lines, respectively by the different parameters of the pulses that are applied to the input. For this purpose, pulse simulations with different durations, different growth times and different propagation times, respectively, were performed.

4.4 Conclusions

The differential pair has certain features related to the way it is fed with common mode or differential signal and even and odd modes. The chapter presents the results obtained for the mixed S parameters and the variation of the impedance when feeding with common mode signal and differential signal. The analysis of the transient regime can be performed with circuit methods, if the parameters L, C, G and R of the differential pair are extracted.

Own contributions in this chapter relate to:

- Modeling of a differential pair made on a low loss Rogers 4003 C substrate for high speed PCBs;
- Study of the variation of the parameters of the differential pair with the electromagnetic field method in the case of differential signal and common mode signal feeding, in the band 1-50 GHz;
- Analysis of reflection and transmission parameters in the band 1-50 GHz, depending on the distance between the lines (1.1; 3.1; 5.1; 7.1 and 9.1 mm), when feeding with defferential and common mode signal using mixed S parameters;

- Analysis of the variation of the differential and common impedance in the band 1-50 GHz, depending on the distance between the lines (1.1; 3.1; 5.1; 7.1 and 9.1 mm).
- Determination of the common signal in the case of differential signal feeding and of the differential signal in the case of common mode signal feeding in the band 1-50 GHz, depending on the distance between the lines (1.1; 3.1; 5.1; 5.1; 7, 1 and 9.1 mm).
- Extraction of the distributed parameters (L, C, G, R), realization of the equivalent scheme with concentrated constants and making the simulations in the time domain for the analysis of the transient regime.

5. Determination of radiated field by vias and microstrip lines in digital circuits and systems

5.1 Introduction

Radiation-transmitted electromagnetic interferences become significant as the operating frequency increases [52]. As a result, increasing the clock frequency increases the transmission line effect on the various traces that provide the necessary connections between different circuits arranged on a printed circuit board. Under these conditions, as the operating frequency of digital systems increases, the electromagnetic compatibility analyses performed at the design stage must be as accurate and detailed as possible. Otherwise, the costs incurred in meeting electromagnetic compatibility requirements (such as shielding, remote separation, etc.) will be much higher. Standards for interference levels and sensitivities / immunity for different types of equipment also need to be revised/supplemented [53]. These standards currently provide the reference levels and the methods for measuring the electromagnetic compatibility parameters up to frequencies between 1 and 6 GHz.

The main sources of the interferences transmitted through radiation are [25] [34]:

1. Horizontal traces made on integrated circuit boards, which ensure the connection between different elements of the respective equipment.
2. Transitions from one layer to another. These vias are used to transmit signals between layers, but also to transmit the ground plane or supply voltage.
3. Combinations between horizontal traces and vias [57].
4. Slots made in the ground plane. These slots are characterized by the fact that one of the dimensions is much smaller than the other.
5. Radiant surfaces. They are characterized by the fact that the two sides have comparable dimensions. They have the same usage as the slots, but they also appear in the case of the housings of different electronic devices.
6. Loops made in the form of a conductive path or as slots. They can be circular, elliptical or rectangular.

5.2 Determination of the field radiated by a linear, infinitesimal radiation source

Electromagnetic phenomena are described by Maxwell's equations which express the interdependencies between the electromagnetic parameters of the environment, dielectric permittivity, conductivity and magnetic permeability, and the quantities that characterize the electromagnetic field, electric field strength $\overline{E}$, magnetic field strength $\overline{H}$, electric induction $\overline{D}$, magnetic induction $\overline{B}$, and volume load (ρ_v).

It is considered that a conductor of length L is placed along the axis Oz and is fed with a current $I_0e^{j\omega t}$. If the diameter of the conductor is denoted by d_c, the expression of the current density in the cross section results:

$$\overline{J}\left(t-r/c\right)=\frac{\overline{I}}{\frac{\pi d_c^{\,2}}{4}}=\frac{\overline{I}_0 e^{j\omega\left(t-r/c\right)}}{\frac{\pi d_c^{\,2}}{4}}\ , \tag{5.26}$$

In the remote or radiation area where the terms that depend on $1/r^2$ and $1/r^3$ can be neglected in relation to those that depend on 1/r, the following relations are obtained:

$$\begin{cases} E_\theta=\dfrac{1}{4\pi\varepsilon}\left(\dfrac{j\omega}{rc^2}+\dfrac{1}{r^2c}+\dfrac{1}{j\omega r^3}\right)I_0e^{j\omega\left(t-r/c\right)}L\sin\theta \\ E_r=\dfrac{1}{4\pi\varepsilon}\left(\dfrac{2}{r^2c}+\dfrac{2}{j\omega r^3}\right)I_0e^{j\omega\left(t-r/c\right)}L\cos\theta \\ E_\varphi=0 \\ H_r=H_\theta=0 \\ H_\varphi=\dfrac{1}{4\pi}\left(\dfrac{j\omega}{rc}\sin\theta+\dfrac{1}{r^2}\sin\theta\right)I_0e^{j\omega\left(t-r/c\right)}L \end{cases}. \tag{5.37}$$

5.3 Determination of the field radiated by a via through the ground plane

Vias through one or more layers of a Printed Circuit Board ensure the transmission of supply voltage or other types of signals between different digital systems [63] [64]. Their frequency behavior influences the parameters of the transmitted signals, and part of the transmitted energy is radiated into the environment around that via. In order to determine the radiated field, different scenarios were analyzed, starting from the hypothesis that the via is open or connected to a line segment of a certain length. The simulations were performed in the 1-40 GHz band.

5.4 Determination of the radiated field by simulations

In order to analyze the behavior of a via, consider a Rogers 4003 C substrate plate, with dimensions: Lm on Ox = 60 mm, lm1 on Oy = 60 mm, ht (via length) = 1,524 mm, De (outer diameter) = 0.46 mm, Dt (via diameter) = 0.2 mm, sh (substrate thickness) = 1.524 mm, Lc (coaxial cable length) = 10 mm, lw (microstrip line width) = 3,1 mm, at the bottom the ground plane, and the via is fed by a coaxial cable with the characteristic impedance of 50 Ω.

Three cases were studied, namely the open via, the via connected to an open microstrip line and the via connected to a microstrip line terminated on a load impedance equal to 50 Ω.

Determination of the field radiated by an open via

The via is fed by a coaxial cable which has the central conductor connected to the via, and the outer conductor to the conductive surface. The power port was defined at the other end of the coaxial cable.

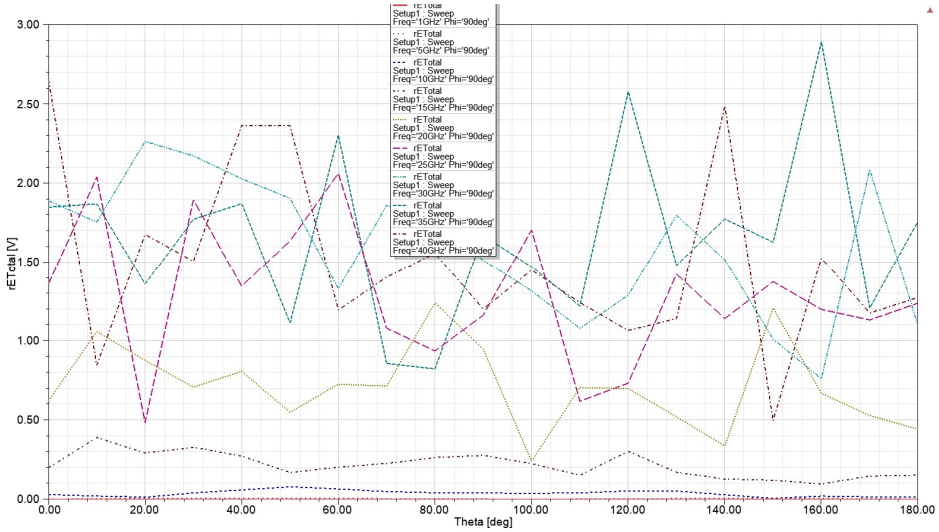

Figure 5.11 Variation of the parameter rE at different frequencies, in the band 1-40 GHz, depending on the angle θ, for $\phi = 90^0$.

On the ordinate of the graph in Figure 5.11 the parameter rE is represented, the field E being expressed in V / m, and r in m. For low frequencies, up to 5 GHz, the value of the radiated field is very small. It increases with frequency, with small variations with the angle θ for f = 10, 15 and 20 GHz. At higher frequencies the dependence of the θ coordinate field is much stronger. At a distance of 10 cm, the largest fields, of the order of 25 V / m, are obtained at the upper end of the band (f = 35-40 GHz).

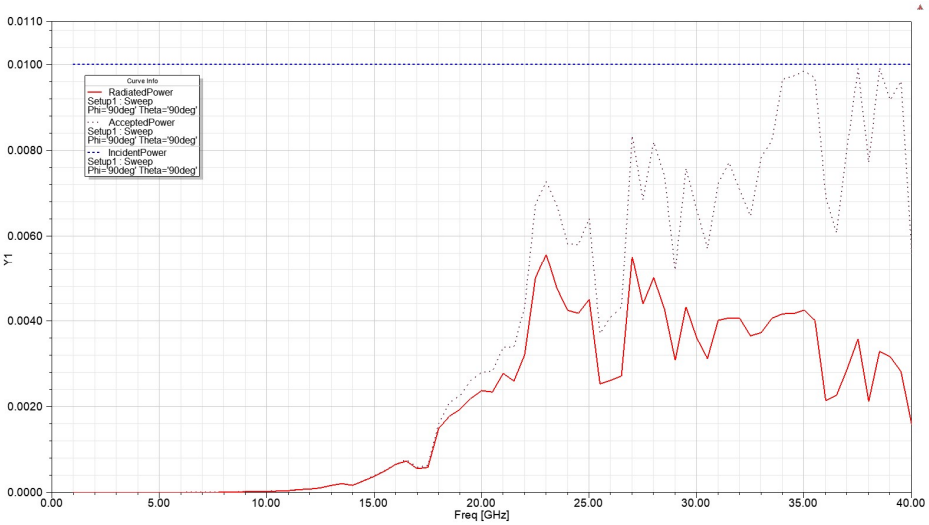

Figure 5.15 Variation of the feeding , antenna and radiated power.

The via is fed by a 10 mm long coaxial cable. The powers shown in Figure 5.15 do not depend on the direction, nevertheless the angles θ and ϕ appear in the legend because they were used as variables in the simulations performed.

The incident power applied to the input of the via is 10 mW and is constant in the 1-40 GHz band. The power transmitted in the via increases with frequency starting with f = 9 GHz, approaching a maximum value of 10 mW in the upper part of the analyzed band. The absorbed and radiated powers by via increase following a parabolic curve in the range of 10-23 GHz, after which the radiated power remains at a value of about 4 mW, while the absorbed power continues to increase.

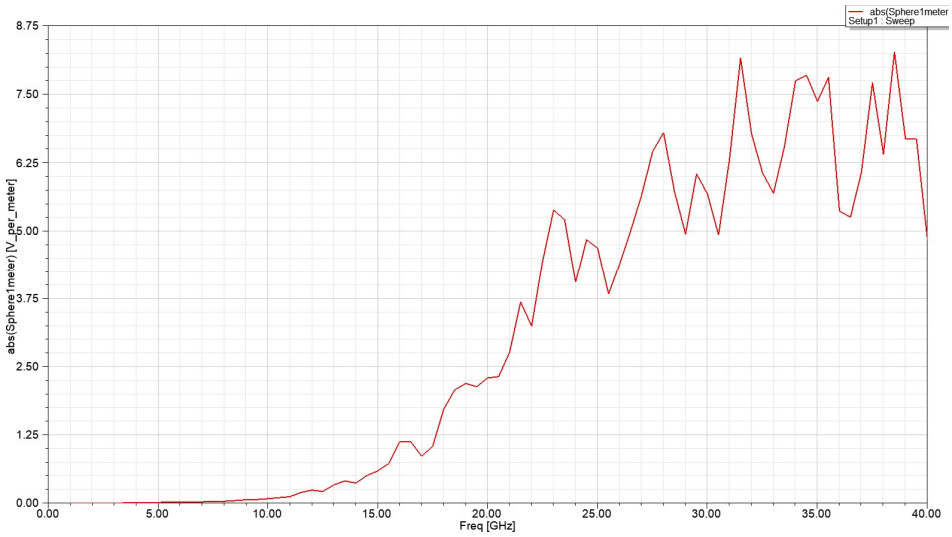

Figure 5.16 Variation of the maximum radiated field as a function of frequency.

The simulation in Figure 5.16 was performed using the "Emission test" option which allows the determination of the maximum value of the emitted field regardless of the direction. This parameter is compared with the value set in the standard corresponding to the field of use of the respective equipment.

Determining the radiated field of a via connected to an open microstrip line

It is considered a via from one layer to another. It is assumed that it is the fed to the lower end by a coaxial cable, and the other end is connected to a microstrip line of length – lL (microstrip line length = 10 mm).

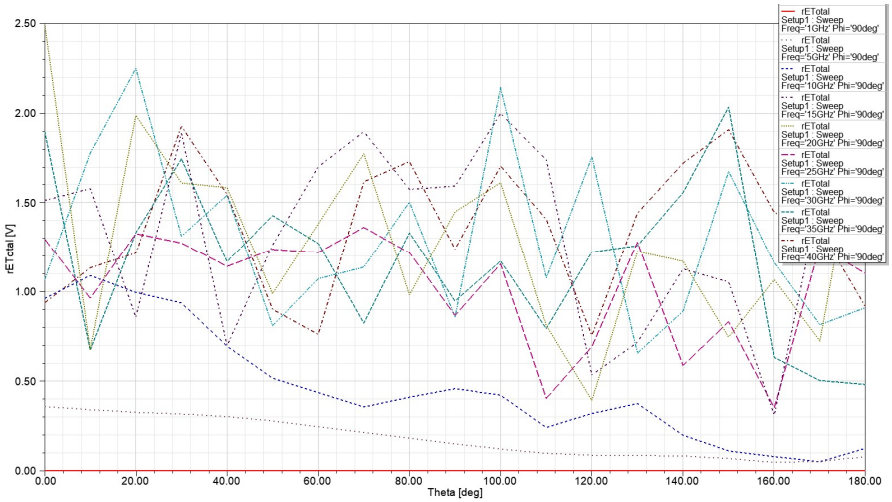

Figure 5.23 Variation of the parameter rE at different frequencies, in the band 1-40 GHz, depending on the angle θ, for $\phi = 90^0$.

Figure 5.23 shows the parameter rE as a function of the angle θ for $\phi = 90^0$. The maximum value of the radiated field is 2.5 V/m and corresponds to the frequency of 20 GHz. For frequencies higher than 10 GHz, the graphs show very similar frequency behavior, but there are large variations in the lower part of the analyzed band, at frequencies of 1, 5 and 10 GHz.

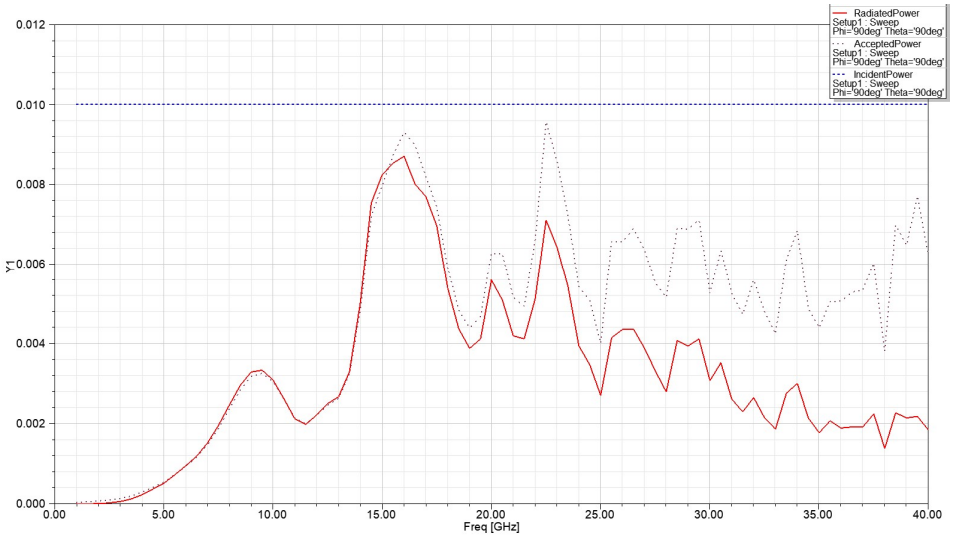

Figure 5.26 Variation of feeding, absorbed and radiated powers.

The via is fed with 10 mW by a coaxial cable, as shown in Figure 5.26. The absorbed power, which depends on the input impedance of the structure, increases till a frequency of 15 GHz (9.2 mW), with a local maximum of 3.5 mW at 10 GHz, after which it oscillates around 6 mW. The radiated power follows the curve described by the absorbed power untill about 20 GHz, after which it decreases to 2 mW at 40 GHz. It is observed that the ratio between radiated and absorbed power decreases from almost 1 to 2/6.2 at 40 GHz.

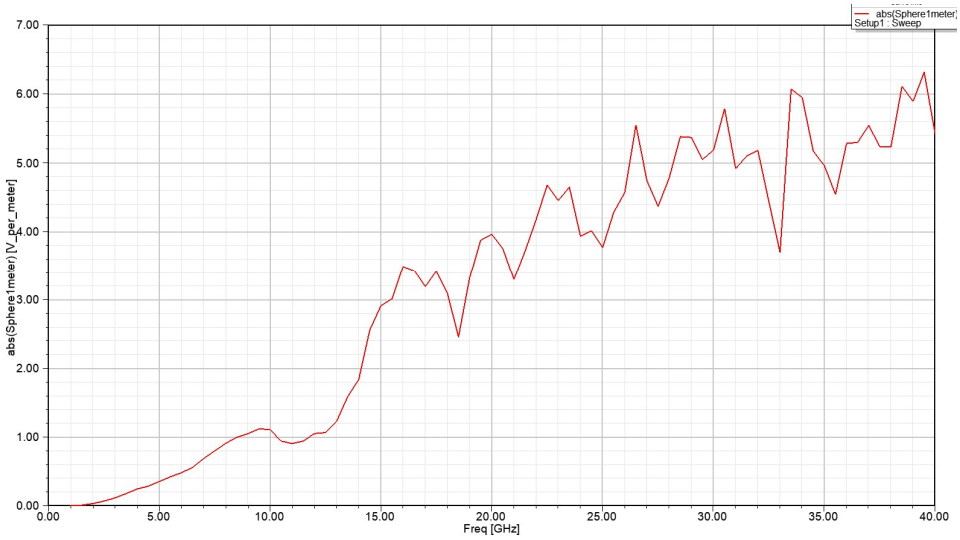

Figure 5.28 Variation of the maximum radiated field as a function of frequency.

The radiated field as a function of frequency, shown in Figure 5.28, ranges from 0 to about 6.4 V/m in the frequency band 1 to 40 GHz. The graph shows the proportionality between the field amplitude and the frequency.

5.5 Conclusions

In the case of GHz operating frequencies, the vias from one layer to another and the connections made on the Printed Circuit Boards become sources of radiation, the electromagnetic energy being transmitted through the substrate and through the air to the neighboring circuits.

The chapter determines the expressions of the fields radiated by the vias and structures formed by horizontal vias and traces, open and connected to a load impedance. The simulations indicate the frequency dependence of the radiated fields and are useful for identifying measures to reduce the interference signals, such as the use of grounded pins, making rejection filters on certain frequencies or shielding to limit the fields transmitted through the substrate, etc.

The main contributions in this chapter are:

- Propose a theoretical model and analytically determine the radiated electromagnetic field by an open via, a via connected to an open microstrip line and a via connected to an matched microstrip line, in the band 1-40 GHz;
- Determining the maximum values of the radiated fields at different distances, for the 3 radiant structures, in the band 1-40 GHz;
- Determining the radiated powers of the 3 configurations encountered in high speed digital circuits;
- Analysis of the electric field radiated by an open via, a via connected to an open *microstrip* line and a via connected to a matched microstrip line, in the band 1-40 GHz in different directions.

6. The study of the field radiated through a slot cut in the ground plane and in the case of a desktop computer

6.1 Introduction

The Printed Circuit Boards contain several layers on which the signal and power traces are made. Depending on the complexity of the system, there may be one or more ground and power planes. Ground planes are made over the entire surface of the PCB or over larger portions of it to provide low inductances for return currents and may have slots of different sizes to secure connectors [72]. Such slots exist both on the front panel for USBs, DVDs, and on the back panel of a desktop computer for power plugs, Internet plugs, expansion card slots, etc. [74]. In order to analyze the frequency behavior of these radiant structures, as well as to analyze their influence on electromagnetic compatibility, the radiated field of a surface is studied, simulations are performed with a slot with the sizes of a slot for an extension card and simulations are performed with a radiation source placed inside an enclosure with conductive walls.

6.2 Radiation of a slot in a conductive surface

In order to analyze the influence that the slots cut in the walls of the enclosures used to fix the various input and output elements, external memory, DVD, USB, CD-ROM, power supply, etc. have, the electromagnetic behavior of a radiant surface of a certain size is first analyzed [77]. A 20X100 mm slot has been chosen (card extension slot on the rear panel of a desktop). The feeding of the slot was made through a port that is at a certain distance from the center of the slot to reduce the input impedance. Figure 6.2 shows the distribution of the electric field in the slot and figure 6.4 shows the parameter rE as a function of frequency.

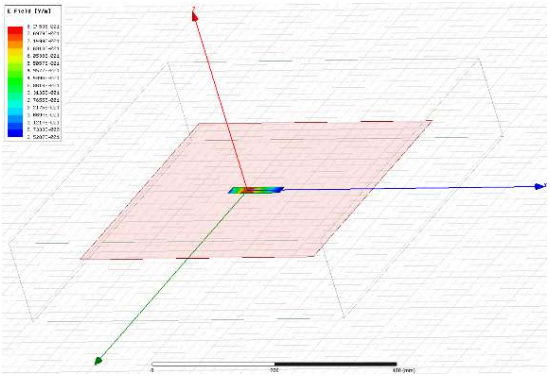

Figure 6.2 The geometry of the radiant structure and the electric field distribution within the slot.

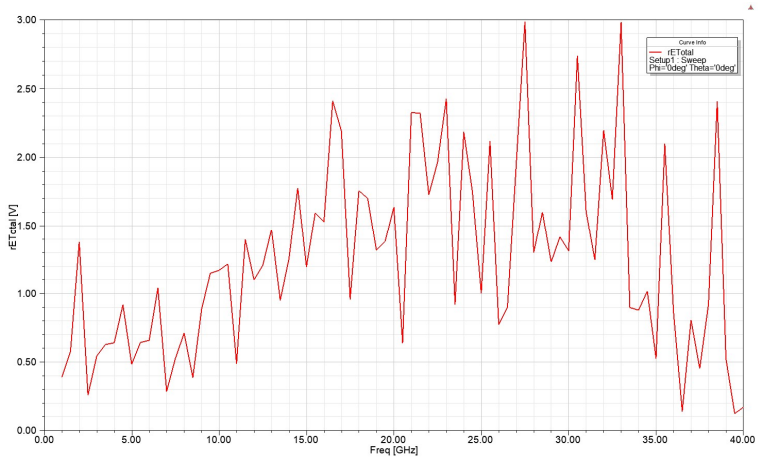

Figure 6.4 Frequency variation of the rE parameter for a slot-card extension slot, in the 1-40 GHz band, for $\theta = 0^0$ and $\phi = 0^0$.

The amplitude of the field radiated by the slot depends on the direction, through the angles $\theta=0^0$ și $\phi=0^0$, on the frequency and on the distance from the slot to the measuring point. For $\theta=0^0$ and $\phi=0^0$, at 1 m, the radiated electric field changes between 0.1 V and 3 V. The highest values are obtained for 27.5 GHz and 34 GHz.

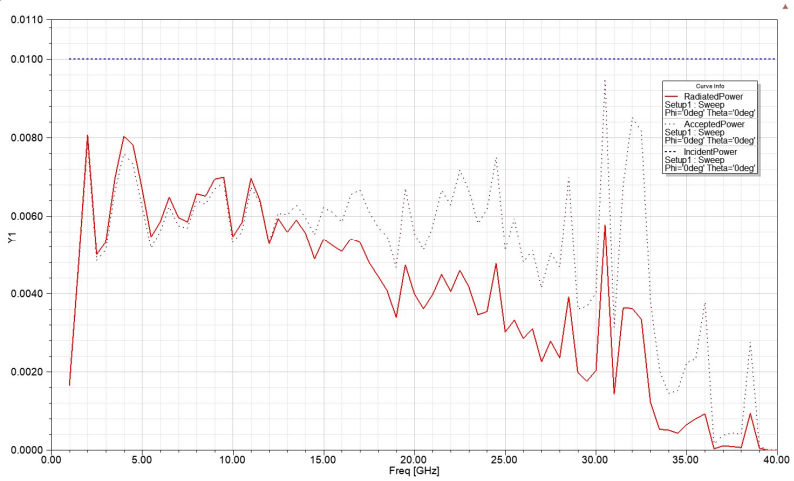

Figure 6.5 Incident, absorbed and radiated powers variation for a slot-card extension slot.

Figure 6.5 shows the absorbed and radiated powers variations, depending on the frequency, assuming that the power applied to the input is constant (10mW). From the graph made in the simulation program, it is observed that in the range 1-12.5 GHz the absorbed and radiated powers are approximately equal. In theory, the radiated power should be less than or equal to the absorbed power. The fact that at some frequencies the radiated power is slightly higher is due to the approximations made by the simulation program. The maximum difference between the two powers is obtained at a frequency of 4 GHz and is 0.004 mW, which represents an error of (0.0004/0.010)X100 = 4%. The radiated power decreases from 8 mW, for f = 2 and 4 GHz, to about 0 mW for f = 40 GHz. The decrease of the radiated power with frequency is explained by the fact that the slot functions as a resonant radiant structure, the efficiency decreases as we move away from the resonant frequency.

6.3 Study of the field produced by an Archimedean spiral radiation source placed inside a desktop enclosure

This chapter examines the electromagnetic behavior of an enclosure inside which there is a radiation source. In order to characterize the fields transmitted outside the enclosure, in the band 1-40 GHz, an Archimedean spiral broadband radiation source it was placed inside the enclosure (Lx- enclosure size on the axis Ox-380 mm, Ly - enclosure size on the axis Oy-220 mm, Lz- enclosure size on the axis Oz-420 mm), which covers a very wide frequency range and works with circular polarization. The enclosure has 0.1 mm thick metal walls. It is considered a desktop enclosure in which a slot of size Lfy - slot size on Oy-100 mm, Lfz - slot size on Oz-20 mm and 0.1 mm was cut. To define the geometric structure, a rectangular reference coordinate system and two relative reference systems were used, CS1 (x = -0.1 mm, y = 100 mm, z = 20 mm) employed for positioning the slot and CS2 (0 mm , 105 mm, 120 mm) for positioning the radiation source. The CS2 coordinate system has the Ox and Oz axes interchanged. Graphical representations were made in the reference coordinate system. The analyzed structure as well as the positioning of the radiation source are presented in figure 6.13. It is observed that the radiation source is aligned with the slot. Figure 6.15 shows the distribution of the electric field.

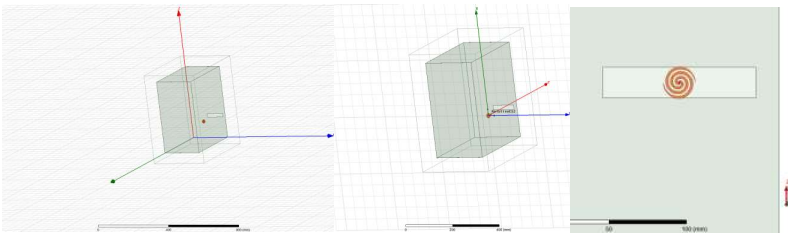

Figure 6.13 Geometric structure analyzed.

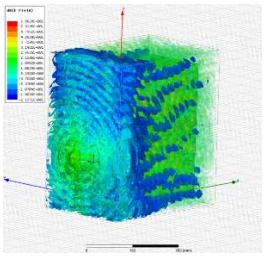

Figure 6.15 Distribution of the E field at 6 GHz.

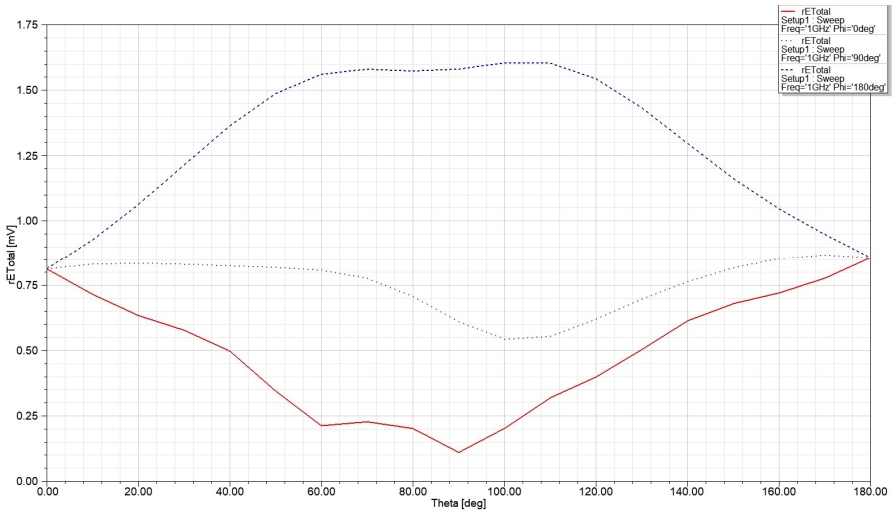

Figure 6.20 Variation of the parameter rE as a function of the angle θ at f = 1 GHz, for ϕ = 0, 90 and 180 degrees.

The electric field in Figure 6.20 is represented in the global coordinate system, in which the angles $\phi = 0$, 90 and 180 degrees indicate the Ox direction towards the inside of the box, the Oy direction in the plane of the box wall and the Ox direction towards the outside of the box.

At a frequency of 1 GHz, figure 6.20, the maximum value of the field is 1.65 mV/m and corresponds to the angle $\phi = 90$ degrees.

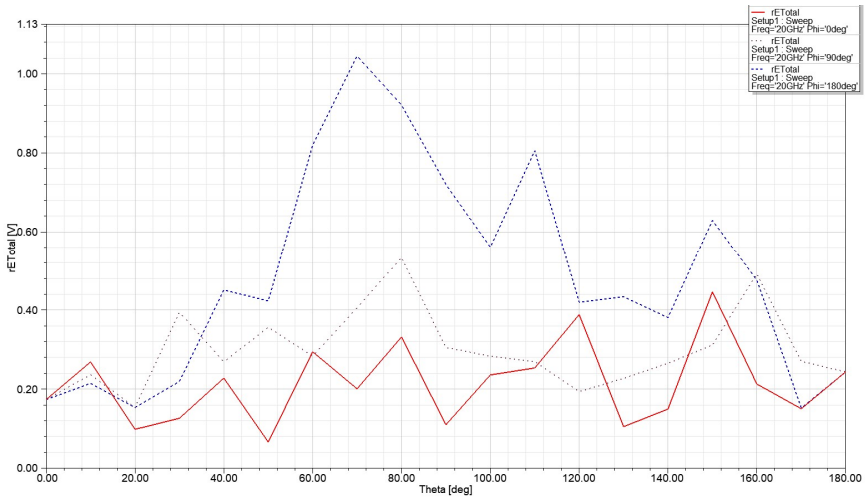

Figure 6.22 Variation of the parameter rE as a function of the angle θ at f = 20 GHz, for ϕ = 0, 90 and 180 degrees.

The distribution of the radiated electric field changes with frequency increasing, a fact illustrated by figure 6.22. At 20 GHz the maximum field amplitude is 1.04 V/m and is obtained for the angle θ equal to 70 degrees. It is noticed that towards the inside of the enclosure and respectively in the plane of the box wall the field has smaller variations.

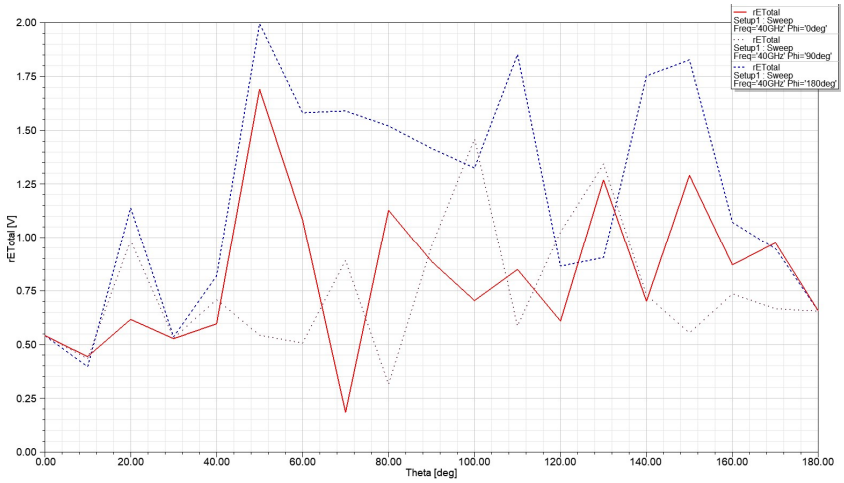

Figure 6.24 Variation of the parameter rE as a function of the angle θ at f = 40GHz, for ϕ = 0, 90 and 180 degrees.

The variation of the radiated electric field at 40 GHz is represented in figure 6.24. The maximum amplitude of the field is 2 V/m and corresponds to an angle θ of 70^0. As in the previous case, the radiated fields in the three analyzed cases have comparable amplitudes.

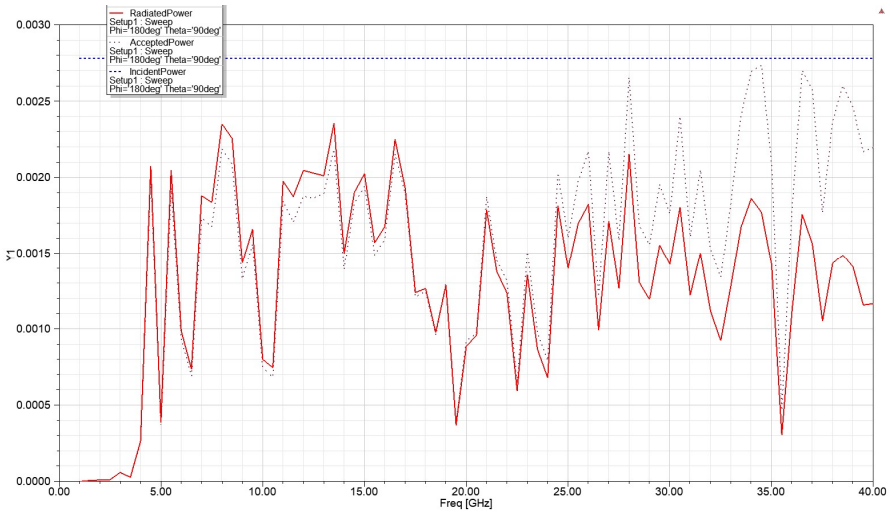

Figure 6.26 Variation of the feeding, absorbed and radiated power.

Figure 6.26 shows the variation of powers assuming that the radiant element inside the enclosure is fed with a power of 0.010 W. The power with which the radiant surface cut into the wall of the rear panel is fed is approximately 0.0028 W. Part of this power is absorbed by the *slot* and part is reflected. The radiated power is shown in red and varies in the range 0-0.00235 W. The graph above shows that the radiated power of the expansion card slot is low to a frequency of 3.5 GHz, then reaches two maximum, 0.00205 W at 4.5 and 5.5 GHz. Following is a frequency band between 6.5 GHz and 10.5 GHz, in which the radiated power has a lobe with a maximum value of 0.00235 W. In the range of 11-17.5 GHz the power varies around 0.0017 W, has a minimum of 0.0004 W at 19.5 GHz and then varies around 0.0015 W to 40 GHz. Starting at f = 24.5 GHz, there is a significant difference between the radiated power and the absorbed power.

6.4 Conclusions

The chapter presented theoretical aspects regarding the determination of the field radiated by a slot cut in a conductive surface, which can be the ground plane of the Printed Circuit Board, or the wall of an enclosure in which the respective digital system operates. The fields were determined, in certain hypotheses, by analytical calculation, but also by simulations performed with a specialized program for calculating the electromagnetic field. The analysis of the electromagnetic compatibility in the case of desktop enclosures must be performed from the perspective of interference transmitted externally through various slots in the enclosure for input-output devices, power plugs for USB plugs and extension cards. In the chapter, the fields radiated outside the enclosure by a slot the size of an extension card slot were determined by simulation. In the simulations performed, a radiation source such as *Archimedean* spiral was used, which was placed inside the enclosure. This type of radiation source has the advantage that it works with circular polarization, therefore it allows the excitation of some slots or conductors randomly arranged in space.

Own contributions in this chapter relate to:

- Analytical determination of the field radiated by a slot with the dimensions of a card extension slot with a certain distribution of the electromagnetic field on the radiant surface, in the band 1-40 GHz;

- Analysis of the power absorbed by the slot and the radiated one, assuming that a power of 10 mW is applied to the input, in the band 1-40 GHz;
- Determination of the maximum radiated field at different distances depending on the frequency, in the band 1-40 GHz;
- Determination of the radiated field at different frequencies in the band 1-40 GHz, depending on the angle θ, measured in relation to an axis perpendicular to the plane of the slot, for different values of the angle ϕ.
- Defining a configuration consisting of a desktop enclosure with a slot in the rear panel and an Archimedean spiral radiation source located inside the enclosure to determine the radiated field outside the enclosure;
- Determination by simulations of the maximum radiated field outside the enclosure, in the band 1-40 GHz;
- Determination by simulations of the maximum radiated field outside the enclosure, in the band 1-40 GHz, in the near field at 10 mm and in the far field at 150 mm from the slot;
- Analysis of the variation of the radiated electric field, at different frequencies, depending on the angle θ, in the plane of the slot and in a plane perpendicular to it;
- Determination of the incident power on the slot, the absorbed power and the radiated power in the 1-40 GHz band.

7. Experimental results

7.1 Coupling signal measurement

In order to compare the results obtained by simulations with those determined by measurements, several Printed Circuit Boards with 3 traces arranged at a distance of 8.1 mm were designed. The substrate used is Rogers 4003 C, and the width was calculated for an impedance of 50 ohms. The three combinations were made in two variants, with a continuous ground plane and a slot in the ground plane with a width of 3 mm, arranged perpendicular to the respective traces. Ports are numbered 1-2 for line 1, 3-4 for line 2 and 5-6 for line 3.

The simulations performed in the case of the 3 lines arranged at a distance of 2.7 trace width from each other, with a 3 mm slot arranged perpendicular to the 3 lines in the central area, shown in Figure 7.6, indicate an increase in the attenuation and an increase in the coupling at the near and far ends. These variations are due to changes in the currents in the ground plane (which bypass the respective slot) and excitation of the slot.

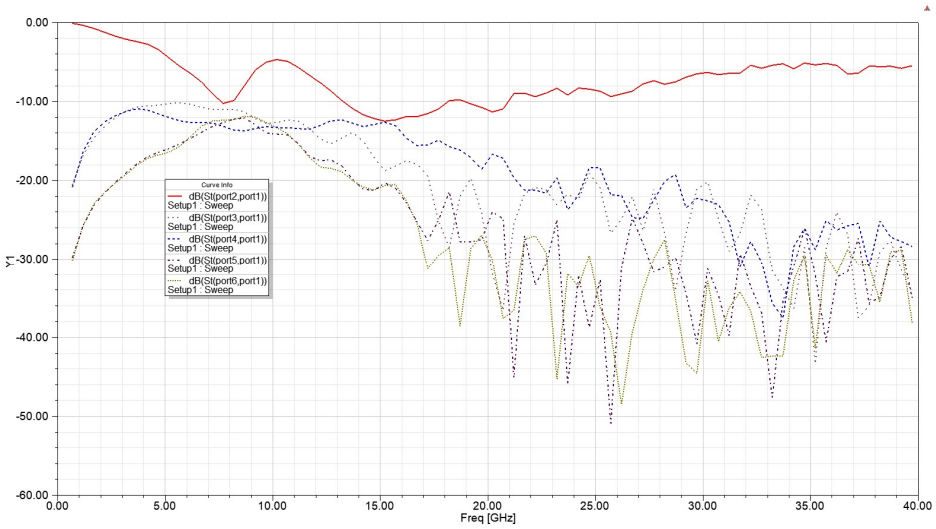

Figure 7.6 Transmission and coupling parameters at near and far ends obtained by simulations for 3 microstrip lines, with slot in the ground plane and the distance between the lines of 2.7lw.

The attenuation, S_{21}, no longer has a linear dependence as in the case of the continuous ground plane, but rises sharply around the 5 GHz frequency and stays around -10 dB to 26 GHz, then the S_{21} drops to -6 dB. At the same time, in the 0.7 -24 GHz band, the S_{41} increases from about -25 dB to an average value of -15 dB, and the S_{61} is much larger and varies in the opposite direction compared to the case with no slot in the ground plane, in the band 0.7-18 GHz.

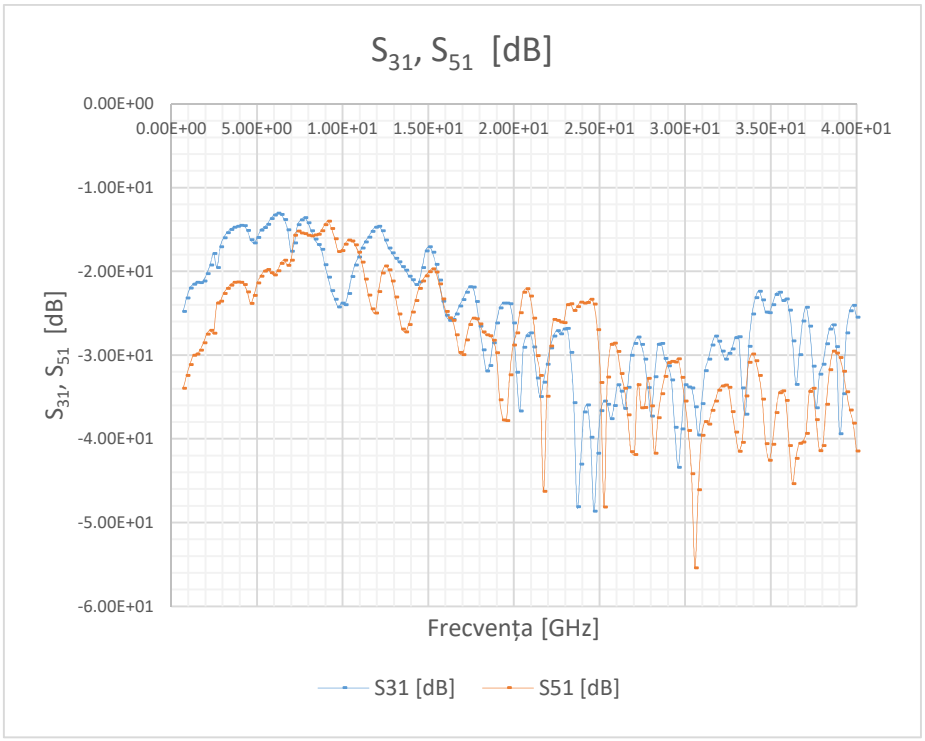

Figure 7.7 Variation of coupling parameters (S_{31} and S_{51}) at the close ends of the 3 microstrip lines with the distance between the lines of 2.7 lw and a slot with a width of 3 mm practiced in the central area of the lines.

The measured values of parameters S_{31} and S_{51} indicate a coupling at the near ends, between lines 1-2 and 1-3, higher than that obtained from the simulations, the difference being of the order of decibels.

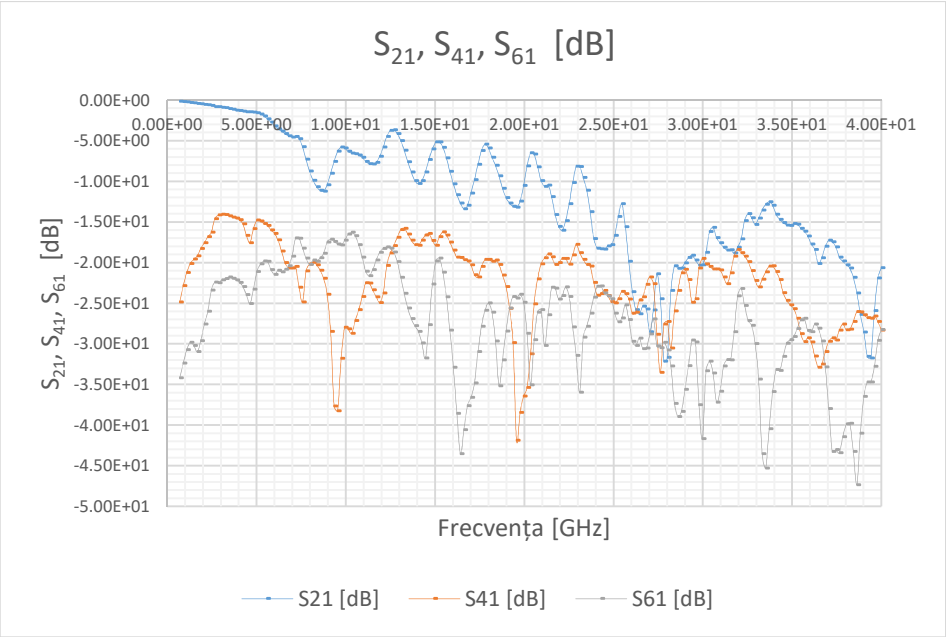

Figure 7.8 Variation of attenuation (S_{21}) and coupling parameters (S_{41} and S_{61}) at the far ends of the 3 microstrip lines with a line spacing of 2.7 lw and a 3 mm wide slot in the center of the lines.

The attenuation characterized by parameter S_{21} is higher in the case of the measured plate. The measured S_{41} has a faster variation than the one obtained by simulations, being present 2 minimums at 9.5 GHz (-36 dB) and at 19.5 GHz (-44 dB). The curve described by the measured S_{61} is close to that generated by simulations, but with an additional attenuation of about 6 dB.

7.2 Determination of the radiated field by measurements

The measurement of the radiated field by a via, respectively by a via connected to an open microstrip line or on an matched load, can be done by connecting a port of the vector analyzer to a radiation source with known parameters, and the other port to the via or the line to be characterized. The available radiation sources were a horn antenna and 2 log-periodic antennas. As a result, measurements were made using these antennas as a reference. They partially cover the band 0.7-40 GHz, so the measurements were made using the horn antenna as a radiation source operating up to 40 GHz. The data measured in the horn-via/microstrip line antenna configuration were compared with those acquired in the horn-periodic antenna-log-periodic antenna configuration.

The practical determinations were made in the case of opon and loaded, as well as a via connected to a microstrip line.

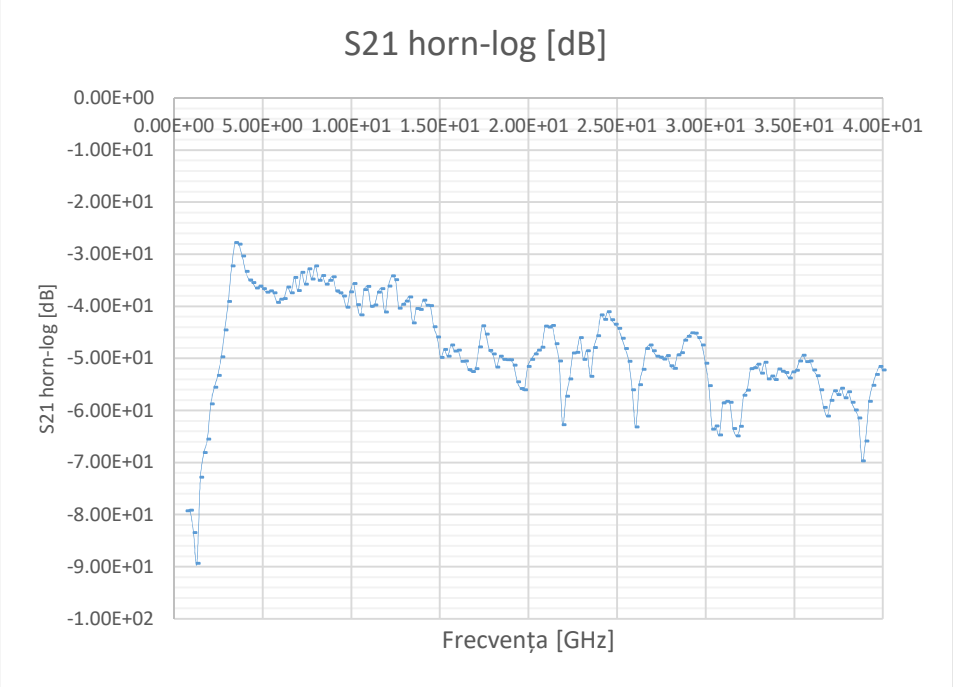

Figure 7.10 Variation of the transmission parameter S_{21} in the horn-logperiodic antennas configuration in the band 0.7-40 GHz.

Figure 7.10 shows the frequency behavior of this ensemble. In the 3-40 GHz band, the average signal level decreases from -30 dB to about -65 dB. As the horn antenna has very weak radiation properties in the band 0.7 -3 GHz, as can be seen in Figure 7.10, the data acuired in the band 0.7-3 GHz have been removed.

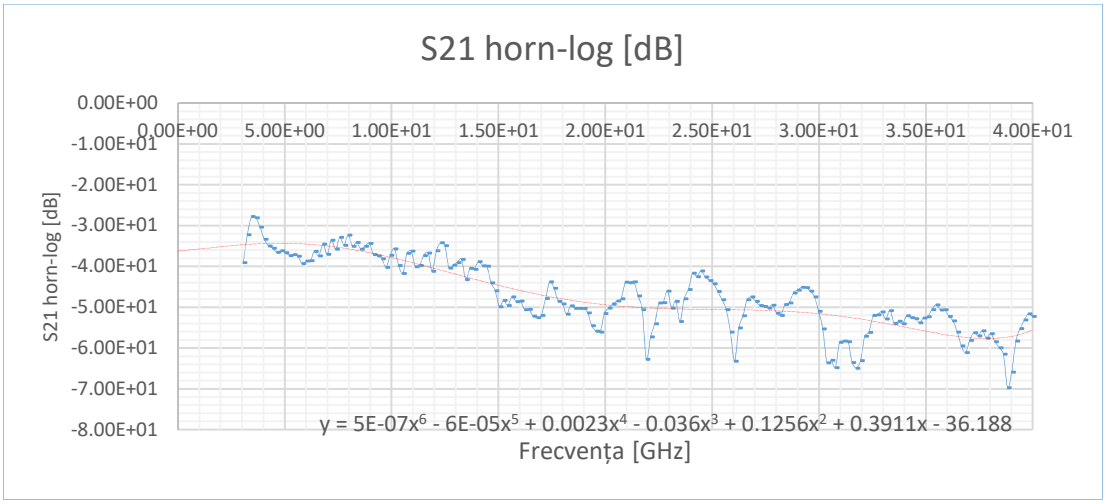

Figure 7.11 Variation of transmission parameter S_{21} in the horn-logperiodic antennas configuration in the 3-40 GHz band.

If we approximate this variation with a polynomial of degree 6 the variation is from -35 dB to -58 dB.

To analyze the influence of a via on the radiated signal, the parameter S_{21} of a via connected to an open microstrip line was measured, and the results were compared with those determined in the case of the open microstrip line.

In the case of the structure consisting of a via connected to the microstrip line, shown in Figure 7.16, the radiated signal varies depending on the frequency between -40 dB and -65 dB.

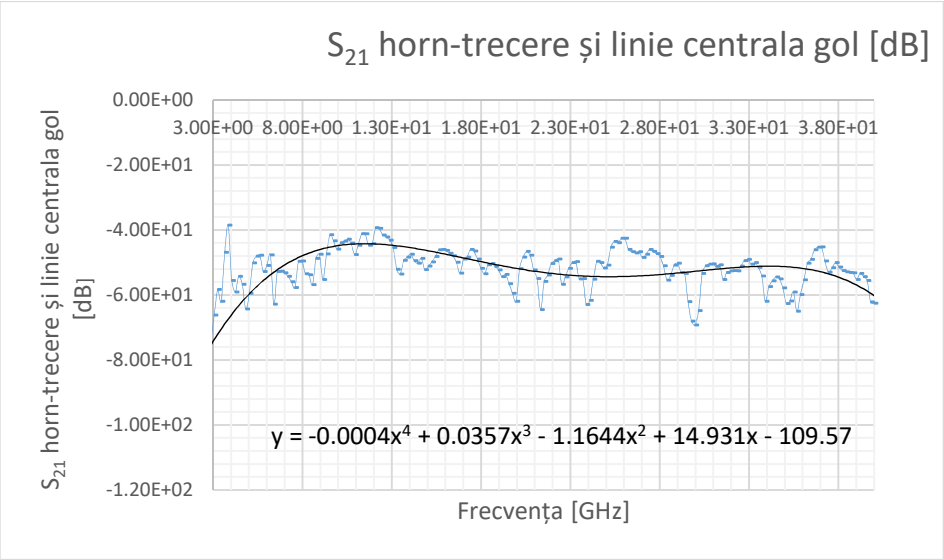

Figure 7.16 Variation of parameter S_{21} in the horn antenna –via connected to an open microstrip line configuration.

Figure 7.17 shows the difference between S_{21} measured in the horn- open line configuration and S_{21} measured in the horn-via and open line configuration.

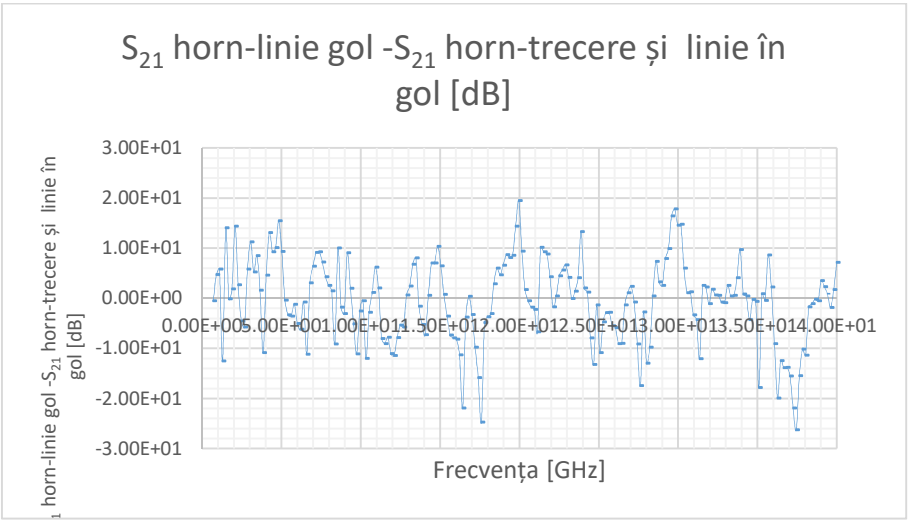

Figure 7.17 The difference between parameter S_{21} measured in open microstrip line and open via configuration connected to a open ended line.

The influence of the via on the radiated signal can be analyzed from figure 7.17. It can be seen that there are variations in the radiated signal of up to 26 dB (37.5 GHz).

7.3 Measurement of the radiated field outside an enclosure

The radiation properties of a rectangular slot cut the rear panel of a desktop enclosure were determined by measurements using a Rohde Schwarz two-channel vector analyzer operating in the 10 MHz-40 GHz band. The distance between the radiation source and

the receiving antenna was set to 60 cm, taking into account the power of the equipment (maximum 8 dBm for calibration). The two antennas work with linear polarization with the electric field vector parallel to the ground surface.

The log-periodic antennas work with linear polarization, and the excitation of the slot was done with the electric field perpendicular to the larger dimension.

The graph in figure 7.24 shows the frequency dependence of the signal transmitted in the free space, in the horn antenna -logperiodic antenna configuration. It is observed that in the band 0.7-3.5 GHz the level of the transmission parameter is lower due to the horn antenna (4-40 GHz).

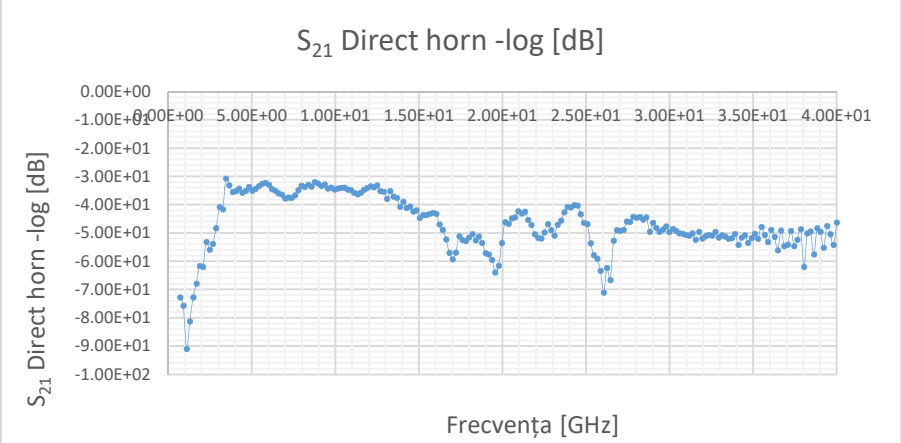

Figure 7.24 Variation of transmission parameter S_{21} in the horn-logperiodic antennas configuration, in the free space (direct).

The signal measured with the horn antenna inside the desktop enclosure has a variation similar to that measured in the free space, however, in some frequency bands, the differences illustrated in figure 7.25 appear.

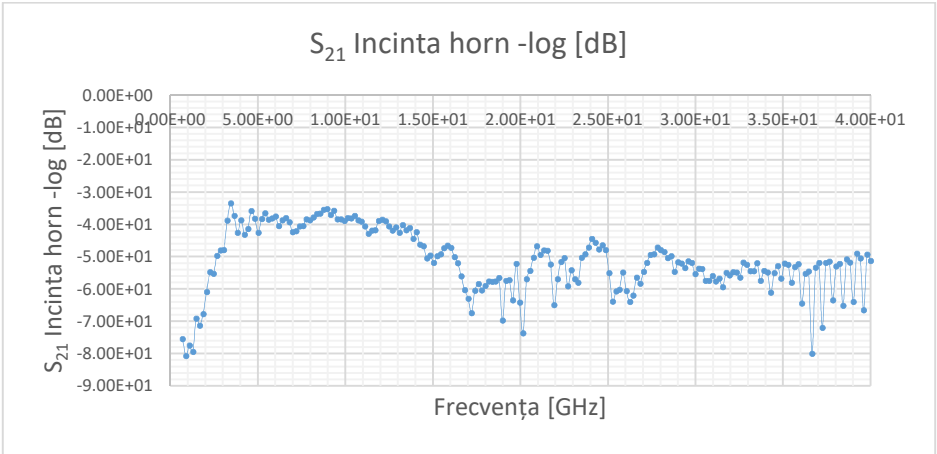

Figure 7.25 Variation of transmission parameter S_{21} in the horn-logperiodic antennas configuration, with the horn antenna in the enclosure.

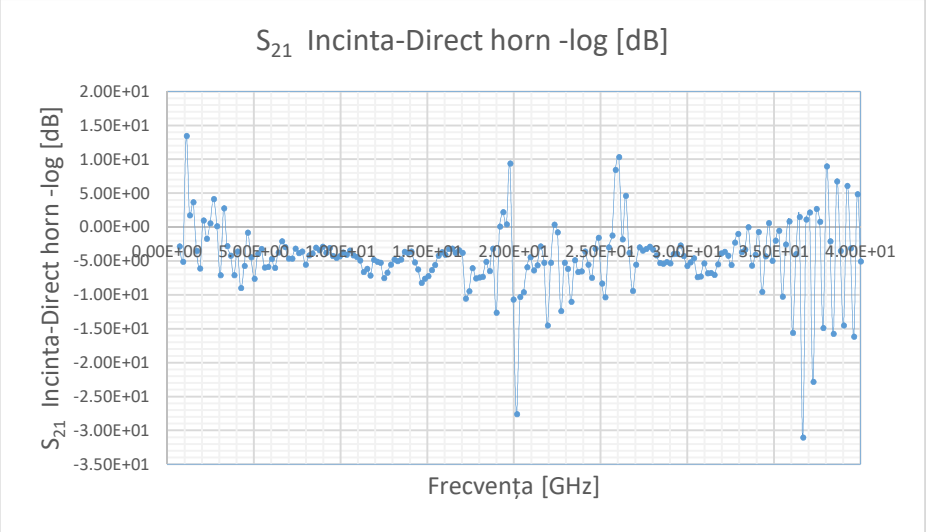

Figure 7.26 The difference between the transmission parameters S_{21}, in the horn-logperiodic antennas configuration, measured with an one antenna within the enclosure and directly.

After processing the measured data in the two configurations, in the free space and with the horn antenna inside the enclosure, the graph from figure 7.26 was obtained. There are 2 bands 19-20 GHz and 25.5-26.5 GHz in which the slot radiates outside the enclosure. The first part of the graph, between 1 and 3 GHz, cannot be taken into account due to the frequency behavior of the horn antenna. Also, in the 33-40 GHz band the very fast variations are produced by the multiple reflections of the enclosure walls.

7.3 Conclusions

The practical experiments carried out in the doctoral thesis aimed at performing measurements in three directions: measuring the coupling signals at the near and far ends in the case of three microstrip lines, measuring the field radiated by open and matched microstrip lines with a length of 60 mm, respectively the field radiated by a via and a open line, the measurement of the radiated field through a slot cut in the rear panel of a desktop enclosure. In order to perform the above mentioned experiments, Printed Circuit Boards with Rogers 4003 C substrate were made, with and without a slot in the ground plane. The practical determinations were performed for 3 microstrip lines arranged at a distance of 2.7lw, the S parameters being determined by simulations and then by measurements. The microstrip lines were also used to measure the radiated field. A Rohde Schwarz vector analyzer in the 0.7-40 GHz band was used for this purpose. To determine the field transmitted through a slot of the size of a card extension slot, a cardboard desktop enclosure was made which was covered with foil. The radiation source, placed inside, was connected to one port of the generator, and the receiving antenna was connected to the other port. Log-periodic and horn antennas were used to perform the measurements.

The main contributions in this chapter are:

- Defining the scenarios for measuring coupling, transmission and reflection parameters, for measuring the radiated field by an open and loaded microstrip line and by a via connected to an open line;
- Design of PCBs with and without a slot for their practical realization;

- Performing the simulations for the 3 microstrip lines and determining all the parameters of reflection, transmission and coupling, in the band 1-40 GHz;
- Measuring the above mentioned parameters with the help of the vector analyzer and comparing the results obtained by simulations with the measured ones.
- Measuring radiated fields by different configurations encountered in high speed digital circuits (1-40 GHz);
- Measuring the radiated field by a slot cut in the rear panel of a desktop computer in the 1-40 GHz band.

8. Conclusions

8.1 Obtained results

The doctoral thesis is organized on 8 chapters and a bibliography. Chapter 1 describes the main trends in the electronic equipment market, highlighting the orientation towards personal use equipment, which leads to an increase in the density of applications employed in a certain space and to an increased in risks from the perspective of electromagnetic compatibility. The electronics industry's response to the demands of increasing data transfer rates, diversifying applications, and ensuring mobility has consisted of devices operating at ever higher frequencies, miniaturization of integrated circuits, parallel processing, and voltage reduction of the power supply. This introductory chapter also presents the objectives of the doctoral thesis and a brief description of the thesis chapters.

Chapter 2, Spectral characterization of digital signals, is intended for the spectral analysis of signals transmitted in digital circuits and systems. The data and command/control signals used in digital systems are in the form of trapezoidal pulses. Aspects of electromagnetic compatibility are intrinsically related to frequency, so in this chapter the band of digital signals is analyzed. The determination of the maximum frequency in the spectrum was performed both by calculus and by simulations.

Chapter 3, The study of the coupling between connections among circuits and digital systems using the electromagnetic field method, analyzes the coupling between connections made in microstrip technology on a low-loss substrate (Rogers 4003 C). The coupling signals were evaluated based on the coupling parameter (S_{ij}) at the near and far ends. Simulations performed in the 0.5-50 GHz band indicate an increase in reflections with frequency from about -40 dB at 0.5 GHz to -12 dB at 50 GHz.

Chapter 4, Analysis of microstrip lines fed with differential signals, made on Rogers 4003 C microwave substrate, studies the differential lines made in microstrip technology. The analysis of the differential pair was performed in the frequency range, in the band 0.5 -50 GHz. The reflection and transmission parameters were determined by simulations in the case of differential feeding for differential and common signals, as well as in the case of common mode sfeeding. The last part of this chapter is dedicated to the time domain analysis of the differential pair. For this purpose, for different frequencies, the equivalent parameters of the line with concentrated constants were extracted based on the simulations performed with the electromagnetic field method.

In Chapter 5, Determining the fields radiated by vias and microstrip lines in digital circuits and systems, the electromagnetic fields radiated by a via, a via connected to an open microstrip line, and a via connected to a matched microstrip line are discussed. The results obtained through simulations indicate a significant variation of the intensity of the radiated electric field depending on the analyzed configuration and angular coordinations.

Next chapter, The study of the field radiated through a practical slot in the ground plane and in the case of a desktop computer, analyzes the electromagnetic interference transmitted by radiation by slots cut in the ground plane or in the housing of a desktop computer. In the first part of the chapter the relations for the radiated electric field are determined, in the hypothesis that on the slot there is a certain distribution of the electromagnetic field. The next section of this chapter determines by simulations the radiated electric field, highlighting its dependence on frequency and angular coordinates. The last part of Chapter 6 is dedicated to the analysis of the field radiated by a slot, having the size of a slot for an extension card, cut in the case of a desktop computer.

Chapter 7, Experimental Results, describes the practical experiments performed to determine the coupling between 2 and 3 transmission lines, with and without a slot in the ground plane. Also, the fields radiated by different connection configurations that ensure the transmission of signals in digital systems have been determined. The last part of this chapter is dedicated to the study of the electromagnetic field transmitted through a slot outside to a metal desktop enclosure, inside which there is a radiation source. The measurements were performed with a vector analyzer, in the band 1-40 GHz, and the results are presented in graphical form and compared with those determined by direct measurements. The latter were used as a reference, as there are no articles in the literature with similar experiments.

The next chapter, Conclusions, presents in a shortly the results obtained in the doctoral thesis, the original contributions, the published works and the directions of further development.

8.2 Original contributions

The main contributions to the development of the research topic refer to:

- Bandwith analysis of periodic trapezoidal pulses used for information transmission and command/control in digital circuits and systems (5), (12).
  - Determination of a relationship for calculating the band of trapezoidal signals, $0.609/t_f$, based on the simulations carried out and on the condition that the amplitude of the spectral components of the periodic trapezoidal pulses is 3 dB lower than the amplitude of the spectral components of the periodic rectangular pulses (with the same duration and the same repetition frequency) (5).
- Application of the electromagnetic field method to study the reflection, transmission and coupling parameters for two single *microstrip* lines made on a Rogers 4003C substrate, depending on the distance between the lines (1.1 mm; 3.1 mm; 5.1 mm; 7.1 mm; 9.1 mm), in the 0.5-50 GHz band (3), (5) (6), (7).

- Application of the electromagnetic field method to study the influence of the coupling between two single *microstrip* lines on the input impedance depending on the distance between the lines (1.1 mm; 3.1 mm; 5.1 mm; 7.1 mm; 9.1 mm) and determining the minimum distance of 5.1 mm for the chosen geometric configuration (3), (5).
- Analysis of the dependence of the attenuation of the signal transmitted through a *microstrip* line on the distance between the two *microstrip* lines (1.1 mm; 3.1 mm; 5.1 mm; 7.1 mm; 9.1 mm) and determining the minimum distance of 5 ,1 mm, which provides a maximum attenuation of – 6 dB at the frequency of 50 GHz (3), (6), (7).
- Near-end coupling study, in the 0.5 GHz-50 GHz band, for different distances between the *microstrip* lines: 1.1 mm; 3.1 mm; 5.1 mm; 7.1 mm; 9.1 mm and identifying 3 subbands (0.5 GHz-15 GHz, 15-46 GHz, 46 GHz-50 GHz) where the coupling parameter follows a certain variation curve (3), (6).
- Analysis of the variation of the coupling signal at the far end according to the distance between the microstrip lines, in the 0.5 GHz-50 GHz band, and its division into 4 sub-bands (0.5 GHz – 3 GHz, 3 GHz – 26 GHz, 26-46 GHz and 46- 50 GHz) where the coupling signal varies similarly (3), (6), (7).

• Application of the electromagnetic field method and the use of small distribution parameters to study the behavior of a differential pair of *microstrip* lines made on a Rogers 4003C substrate, in the 0.5 GHz-50 GHz band, for different distances between the *microstrip* lines: 1.1 mm; 3.1 mm; 5.1 mm; 7.1 mm and 9.1 mm (2), (3).

- Determining the reflection parameters in the case of feeding the differential pair with a differential signal and highlighting its advantages, namely the reflection parameter - St(diff1,diff1) of approximately -45 dB and St(comm1,diff1) with values between -70 dB and -50 dB, compared to values between -40 dB and -10 dB for single lines (2).
- Emphasizing, based on the simulations performed with the electromagnetic field method, the reduced dependence of the reflection parameters on the distance between the two *microstrip* lines in the case of differential feeding. Thus, the reflection parameter St(diff1,diff1) varies very little with the distance between the lines for the distances: 3.1 mm; 5.1 mm; 7.1 mm and 9.1 mm (less than -40 dB), and in the range 0.5 GHz-20 GHz, for a distance of 1.1 mm it has an average value of -35 dB. The reflection parameter St(comm1,diff1) increases from approximately -70 dB at 0.5 GHz to -50 dB at the frequency of 50 GHz, the curves describing the dependence on the distance between the lines having a similar variation (3), (2).
- Determining the attenuation of the signal transmitted through a differential pair of *microstrip* lines, in the 0.5-50 GHz band, depending on the distance between the lines and highlighting the fact that the attenuation is lower than in the case of a single line (the maximum value of -1.2 dB, at 50 GHz, compared to about -6 dB for a line spacing of 7.1 mm) and that the influence of line spacing is negligible for frequencies above 12 GHz (3), (2).

• Analysis of the differential and common impedances of a differential pair of *microstrip* lines made on a Rogers 4003C substrate, in the 0.5 GHz - 50 GHz band, depending on the distance between the *microstrip* lines: 1.1 mm; 3.1 mm; 5.1 mm; 7.1mm and 9.1mm (2):

- In the frequency band 0.5 GHz - 8 GHz the differential impedance is approximately constant, but the values differ depending on the distance between the lines (approximately 97 ohms for the distances of 5.1 mm; 7.1 mm and 9.1 mm, 90 of ohms for 3.1mm and 74 ohms for 1.1mm spacing.
- In the frequency band 8 GHz - 50 GHz the differential impedance increases approximately linearly to 158 ohms, 152 and 150 ohms respectively, for the distances mentioned above.
- The common impedance varies approximately linearly from 25 ohms, for distances of 5.1 mm; 7.1 mm and 9.1 mm, at 39 ohms, and from 26.5 to 39.50 ohms for the 3.1 mm distance, and from 29 to 42 ohms for the 1.1 mm.

• Analysis in the time domain of the differential pair of microstrip lines based on the parameters calculated with the electromagnetic field method in the band 0.5 GHz-50 GHz (5).

- Evaluation through simulations in Ansoft Nexxim of the influence of the differential pair on the signals, with different parameters, applied to the input of the scheme built with the parameters extracted using the HFSS simulation program, for 3 frequencies: 1.3 GHz, 3.6 GHz and 10 GHz (5), (7):
  - For 1.3 GHz the oscillations are about 10% of the pulse amplitude value and the front time increases from 54 ps to about 70 ps.
  - For 3.6 GHz the oscillations are about 40% of the pulse amplitude value and the front time increases from 20 ps to about 70 ps.
  - For 10 GHz the oscillations are about 60% of the pulse amplitude value and the front time increases from 10 ps to about 80 ps.

• Theoretical and experimental analysis of the reflection, transmission and coupling parameters of two structures consisting of 3 *microstrip* lines made on a Rogers 4003 C substrate with a continuous ground plane and with a slit made in the ground plane, in the 0.5 band GHz-50 GHz.

- Modeling in HFSS and practical realization of 2 plates on a Rogers 4003 C substrate with 3 *microstrip* lines arranged at a distance of 2.7xpath width, with and without a slot in the ground plane.
- Analysis of the influence of a slot in the ground plane on the reflected, transmitted and coupling signals in the 0.5 GHz-50 GHz band (4), (9).

• Study of the electromagnetic field radiated by a via and a via connected to a *microstrip* line, carried out on a Rogers 4003C substrate, open, respectively terminated on a matched load, in the 1-40 GHz band using a model based on the image method (1).

- Determination of the power radiated by a via as a function of frequency (1-40 GHz) and showing that it increases in the frequency range 10-23 GHz from 0 mW to 5.6 mW, and in the range 23-40 GHz oscillates around 4 mW (supply power is 10 mW). The maximum radiated field varies parabolically

in the frequency range 10-40 GHz, reaching a maximum value of 8.25 V/m at 31.5 GHz and 38.5 GHz.

- Analysis of the radiated electromagnetic field by a via connected to a open *microstrip* line, in the 1-40 GHz band, and identification of the frequency range 13.5 GHz- 24 GHz where the radiated power is greater than 4 mW, reaching the maximum value of 8.4 mW at the frequency of 16 GHz.
- Study of the electromagnetic field radiated by a microstrip line terminated on Z=50 ohms and highlighting the fact that the power variation is smaller and the 4 mW value is exceeded between 19.5 GHz and 23.5 GHz (1).
- Study of the variation of the electric field radiated by vias and combined structures,vias and microstrip lines, in the 1-40 GHz band, depending on the angular coordinates (1).

• Measurement of the electric field radiated by an open microstrip line, a microstrip line connected to a matched load and a via connected to a open microstrip line using a horn antenna for reception, in the 1-40 GHz band.

- Comparative analysis of the fields radiated by an open microstrip line and a terminated line on a matched load using wide-band horn and log-periodic antennas for reception.

• Performing simulations and determining the radiated electromagnetic power and radiated electric field as a function of frequency (1-40 GHz) for a slot of the size of an expansion card. The radiated power drops from about 8 mW at f=2 GHz to 0 mW at 36.5 GHz.

- Comparing the fields radiated by the expansion card slot-slot and the microstrip line crossing combined structures it is found that the slots radiate a greater amount of energy in the lower part of the band, 1-20 GHz, and the combined structures in the central part 13-24 GHz .
- Determination of the variation of the radiated electric field in the plane of the slot and in a plane perpendicular to the slot in the 1-40 GHz band.

• Performing simulations and determining the distribution of the electric field radiated through an expansion card-sized slot by a radiation source placed inside a desktop-type enclosure at various distances in the 1-40 GHz band. The maximum field value at 10 mm distance is 5.8 V/m (f=4 GHz) and at 150 mm it is 12.4 V/m (36.5 GHz).

- Modeling of an Archimedean spiral type radiation source arranged inside a desktop type enclosure.
- Determination of the transmission power through the slot of an extension card if the radiation source is placed inside the desktop enclosure. The power varies between 0.5 mW and 2.3 mW, having a much smaller variation compared to the other cases analyzed (via and combined structures *microstrip* vias and lines).
- Comparative analysis of the maximum electric fields radiated by the slot of an extension card powered directly and irradiated by a source placed inside the enclosure. The maximum value of the total electric field is 5.4 V/m and

corresponds to the frequency of 37 GHz, in the case of direct feeding, and 1.855 V/m at 31.5 GHz ($\phi=180^0$, $\theta=90^0$), in the case of irradiation by spiral.

• Measurement of the transmitted field through the slot in the back of a desktop enclosure, in the following configurations:

- log-periodic antenna-log-periodic antenna;
- horn antenna-log-periodic antenna.

- Determination of the electric field radiated through the slit using as a reference the direct measurements made for the two analyzed configurations.

8.3 List of publications

1. Mircea Nicolaescu, Victor Croitoru, Leontin Tuță, Radiated Fields by Vias and Matched Microstrip Traces in High Speed PCBs, 14th International Conference on Communications (COMM), Comm 2022, Bucharest, Romania, DOI: 10.1109/COMM54429.2022.9817166, under publication in ISI Proceedings data base - chapters 5 and 7.
2. Mircea Nicolaescu, Victor Croitoru, Mihai Enache, Microstrip Differential Pair Full Wave Electromagnetic Analysis, 14th International Conference on Communications (COMM), Comm 2022, Bucharest, Romania, DOI: 10.1109/COMM54429.2022.9817275, under publication in ISI Proceedings data base - chapter 4.
3. Mircea Nicolaescu, Paul Svasta, Mihai Enache, Full Wave Electromagnetic Analysis of Coupling in High Speed Microstrip Single Ended Lines with Different Separations, 14th International Conference on Communications (COMM), Comm 2022, Bucharest, Romania, DOI: 10.1109/COMM54429.2022.9817234, under publication in ISI Proceedings data base - chapters 3 and 7.
4. Mircea Nicolaescu, Victor Croitoru, Leontin Tuță, Radiation of a Slot in High Speed Digital Systems, Rev. Roum. Sci. Techn. – Électrotechn. et Énerg.- Rev. Roum. Sci. Techn. – Électrotechn. et Énerg.- Vol.67, 3 , pp. 327-330, Bucharest, 2022, WOS:000870731700017 - chapters 6 and 7 .
5. Mircea Nicolaescu, Victor Croitoru, Leontin Tuță, Transient analysis of a microstrip differential pair for high speed Printed Circuit Boards, Rev. Roum. Sci. Techn. – Électrotechn. et Énerg.- Vol.67,2, pp. 167–170, Bucharest, 2022 WOS:000850185600013 – chapters 2 and 4.
6. Nicolaescu, M; Croitoru, V; Tuta, L, Electromagnetic Analysis of Crosstalk in Electronic Digital Modules, 2020 13th International Conference on Communications (COMM), Bucharest, Romania WOS:000612723900082 – chapter 3.
7. Nicolaescu, M; Stoica, D, Two PCB Traces Coupling Analysis, 2020 13th International Conference on Communications (COMM), Bucharest, Romania WOS:000612723900080- chapter 3.
8. Tuta, L; Nicolaescu, M; Rosu, G; Grivei, A; Barbulescu, B, A Robust Adaptive Filtering Method based on Independent Component Analysis (ICA), 13th 2020

13th International Conference on Communications (COMM), Bucharest, Romania, 2020, ISI Proceedings WOS:000612723900010- chapter 8.
9. Buzinu, L, I; Anton, L; Deparateanu, D; Nicolaescu, M, Analysis of an Array of Rectangular Apertures Based on the Active Parameters of its Infinite Extension, 2018 12th International Conference on Communications (COMM), Bucharest, Romania, WOS:000449526000040- chapter 6.
10. Ionut-Valentin Grecu, Mircea Nicolaescu, Automatic Propagation Model Tuning Process in TETRA Networks, 2016 International Conference on COMMUNICATIONS, June 9–11, 2016 Bucharest, Romania, Conference Proceedings ISBN 978-1-4673-8196-3, Part No. CFP1641J-DVD, pag 211-2014, IEEE Xplore, ISI Proceedings WOS:000383221900048- chapter 1.
11. George Cașu, Andrei Kovacs, Mircea Nicolaescu, Alexandra Mocanu, A Comparative Performance Analysis of MIMO-OFDM System over Different Fading Channels, ECAI 2014 - International Conference – 7th Edition Electronics, Computers and Artificial Intelligence, 25 June -27 June, 2015, Bucharest, România, IEEE -Xplore, ISI Proceedings WOS:000383221900048- chapter 1.
12. George Cașu, Mircea Nicolaescu, A Comparative Performance Analysis of Digital Modulation Schemes used in Mobile Radio Systems, Faculty of Electronics and Informatics, International Journal of Advanced Research in Physical Science (IJARPS) Volume 2, Issue 5, May 2015, pp 7-13 ISSN 2349-7874 (Print) & ISSN 2349-7882- chapter 1.
13. Nicolaescu Mircea, Croitoru Victor, Gheorghică Daniel, Securitatea sistemelor de poștă electronică, Al IX-lea Simpozion Național de Informatică, Automatizări și Telecomunicații în Energetică, SIE 2012, pag. 179-185, Sinaia, 24-26 octombrie, 2012.

8.4 Prospects for further development

The development of technologies for the development of electronic devices, miniaturization, increasing the frequency of work, large-scale integration, diversification of applications and increasing the number of those addressed to individual users lead to an agglomeration of radio spectrum and increasing the importance of electromagnetic compatibility which has to be adressed in the initial stages of the development of the digital systems. Knowing the behavior of a digital system in a highly complex electromagnetic environment will be one of the important goals to be pursued by designers. Therefore, frequency and time analyses must be performed rigorously to identify the frequencies at which interferences may be generated, as well as the electromagnetic susceptibility of the equipment. An important direction for the development of the approached topic refers to time domain reflectometry (TDR) which will allow a better knowledge of the transient regimes in digital systems. Another important dimension of the electromagnetic compatibility must take into account the increase in the density of the equipment, which reduces the distance between them. As a result, a direction of the development of the approached subject refers to the study of the behavior of different sources of interference and carrie out the measurements in the near

field. Performing practical determinations in the near field area requires special probes that allow the measurement of electric or magnetic fields without disturbing the electromagnetic field. A third direction of development refers to the analysis of the possibility of recovering the information conveyed in digital systems based on interference transmitted by conduction, by inductive and capacitive coupling or by electromagnetic field.

Bibliography

[1] The International Roadmap for Devices and Systems: 2020- IEEE, https://irds.ieee.org/editions/2020.

[2] Etienne Sicard, Alexandre Boyer. Impact of Technological Trends and Electromagnetic Compatibility of Integrated Circuits. EMC Compo 2019, Oct 2019, Haining, China.

[3] Thierauf Stephen, High-Speed Circuit Board Signal Integrity, Second Edition, Artech House, 2017.

[4] The International Roadmap for Devices and Systems: 2021- IEEE, https://irds.ieee.org/editions/2021.

[5] M. Keating, D. Flynn, R. Aitken, A. Gibbons, and K. Shi, Low Power Methodology Manual for System on Chip Design. Springer, 2007.

[6] Brajesh Kumar Kaushik V. Ramesh Kumar Amalendu Patnaik, Crosstalk in Modern On-Chip Interconnects A FDTD Approach, Springer Science, 2016.

[7] D.D. Rio, I. Gurutzeaga, A. Rezola, J.F. Sevillano, I. Velez, V. Puyal, J.L. Gonzalez-Jimenez, R. Berenguer, A 15–21 GHz I/Q upconverter with an on-chip linearization circuit for 10 Gbps mm-wave links, IEEE Microw. Wirel. Compon. Lett. 27(5), 2017.

[8] S. H. Kulkarni, A. N. Srivastava, and D. Sylvester, A New Algorithm for Improved VDD Assignmentin Low Power Dual VDD Systems, Proc. International Symp. Low Power Design, , pp. 200-205, 2004.

[9] David del Rio, Ainhoa Rezola Juan F. Sevillano, Igone Velez Roc Berenguer, Digitally Assisted, Fully Integrated, Wideband Transmitters for High-Speed Millimeter-Wave Wireless Communication Links, Springer International Publishing, 2019.

[10] Ionut-Valentin Grecu, Mircea Nicolaescu, Automatic Propagation Model Tuning Process in TETRA Networks, International Conference on Communications, June 9–11, Bucharest, Romania, 2016, ISI Proceedings WOS:000383221900048.

[11] Micron® GDDR6 Memory Product Flyer Brief/Flyer (PDF) - 7.3.2019, www.micron.com.

[12] IEC61967-1:2018 : Integrated circuits - Measurement of electromagnetic emissions, 150 kHz to 1 GHz - Part 1: General conditions and definitions, International Standard, International Electrotechnical Commision, Dec. 2018.

[13] IEC62132-1:2015 : Integrated circuits - Measurement of electromagnetic immunity - Part 1: General conditions and definitions, International Standard, International Electrotechnical Commision, Oct. 2015.

[14] IEC 61000-4-4 Electromagnetic Compatibility (EMC)—Part 4-4: Testing and Measurement Techniques—Electrical fast transient/burst immunity test, 2012.

[15] Hanqiao Zhang, Steve Krooswyk, Jeff Ou: High Speed Digital Design. Elsevier Inc., 2015.

[16] Cașu G., Kovacs A., Nicolaescu M., Mocanu A., A Comparative Performance Analysis of MIMO-OFDM System over Different Fading Channels, 7th Edition Electronics, Computers and Artificial Intelligence, ISI Proceedings, 2015, Bucharest, WOS:000383221900048.

[17] George Cașu, Mircea Nicolaescu, A Comparative Performance Analysis of Digital Modulation Schemes used in Mobile Radio Systems, International Journal of Advanced Research in Physical Science , Volume 2, Issue 5, May 2015.

[18] Roza Dastres, Mohsen Soori. A Review in Advanced Digital Signal Processing Systems, International Journal of Electrical and Computer Engineering, 2021.

[19] C. S. H. Kaushik, T. Gautam and V. Elamaran, A tutorial review on discrete Fourier transform with data compression application, Conference on Green Computing Communication and Electrical Engineering (ICGCCEE), pp. 1-6, 2014.

[20] Levent Sevgi, Fourier Transform and Fourier Series, IEEE Electromagnetic Modeling and Simulation, pp.71-94, 2014.

[21] C.R. Paul, Introduction to Electromagnetic Compatibility, 2nd edition, John Wiley, 2005.

[22] Canavero, Flavio G. and Clayton R. Paul, Bandwidth of Digital Waveforms, 2010..

[23] MicroSimPSpice A/D &Basics+-Circuit Analysis Software, User'sGuide, MicroSim Corporation, USA.

[24] B. Sindhura, S. Ashwin, G. Rajkumar, V. Elamaran and M. Sankar, Useful Tips and Tricks on Digital Data Processing with Discrete Fourier Transform, Second International Conference on Computing Methodologies and Communication (ICCMC), 2018.

[25] Bogatin, E., Signal and Power Integrity- Simplified, Prentice Hall, 2018.

[26] G. Jagadeeswar Reddy, T. Jayachandra Prasad, Basics of Electromagnetics and Transmission Lines, CRC Press Taylor & Francis Group, 2020.

[27] Ravish R Singh, Circuit Theory and Transmission Lines, Second Edition, McGraw Hill Education, Green Park Extension, New Delhi, 2016.

[28] Eric Bogatin, Practical guide to transmission line design and characterization for signal integrity applications, Artech House USA, 2020.

[29] Stephen H. Hall, Garrett W. Hall, James A. McCall, High-Speed Digital System Design: A Handbook of Interconnect Theory and Design Practices, Wiley-IEEE Press, September 2000.

[30] S. B. Dhia, M. Ramdani, and E. Sicard, Electromagnetic Compatibility of Integrated Circuits—Techniques for Low Emission and Susceptibility. Springer: Berlin, Germany, 2006.

[31] Terry C. Edwards, Michael B. Steer, Foundations for Microstrip Circuit Design, John Wiley & Sons, 2016.

[32] Resso Mike and Bogatin, Eric Signal Integrity Characterization Techniques, Addie Rose Press, 2019.

[33] Tom Granberg: Handbook of Digital Techniques for High-Speed Design. Prentice Hall, 2004.

[34] Xing-Chang Wei, Modeling and design of electromagnetic compatibility for high-speed printed circuit boards and packaging, CRC Press, Taylor & Francis Group, 2017.

[35] Peter J. Pupalaikis: S-Parameters for Signal Integrity. Cambridge University Press, March 31, 2020.

[36] R. Ianconescu and V. Vulfin, Analysis of lossy multiconductor transmission lines and application of a crosstalk canceling algorithm, Iet Microw Antenna P, 11(3), pp. 394-401,2016.

[37] Douglas Brooks: Signal Integrity Issues and Printed Circuit Board Design. Prentice Hall, October 2012.

[38] Ramesh Garg Inder Bahl Maurizio Bozzi, Microstrip Lines and Slotlines, Artech House, USA, 2013.

[39] Clayton R. Paul, Transmission lines in digital systems for emc practitioners, John Wiley & Sons, Inc., Hoboken, New Jersey, 2012.

[40] Dennis Miller, Designing High-Speed Interconnect Circuits. Intel Press, 2004.

[41] Tzyh-Ghuang Ma, Chao-Wei Wang, Chi-Hui Lai, Ying-Cheng Tseng, Synthesized transmission lines : design, circuit implementation, and phased array applications, NJ : John Wiley & Sons, 2017.

[42] HFSS-user's guide, ANSOFT Corporation, USA.

[43] Nicolaescu, M; Croitoru, V; Tuta, L; Electromagnetic Analysis of Crosstalk in Electronic Digital Modules, 13th International Conference on Communications (COMM), WOS:000612723900082, Bucharest, 2020.

[44] Nicolaescu, M; Stoica, D; Two PCB Traces Coupling Analysis, 13th International Conference on Communications (COMM), WOS:000612723900080, Bucharest, 2020.

[45] Tian et al., Study of Fields Above Differential Microstrip lines for Probe Characterization Application, 12th International Workshop on the Electromagnetic Compatibility of Integrated Circuits (EMC Compo), pp. 234-236, 2019.

[46] James Mears, National Semiconductor application note AN-905.

[47] Stephen Hall, Garrett Hall, James McCall, High-Speed Digital System Design, A Handbook of Interconnect Theory and Design Practices. John Wiley and Sons, Inc. New York, 2000..

[48] T. Watanabe, O. Wada, T. Miyashita and R. Koga, Common Mode Current Generation Caused by Difference of Unbalance of Transmission Lines on a Printed Circuit Board with Narrow Ground Pattern, IEICE Trans. Commun., vol. E83-B(3), pp. 593–599, 2000.

[49] Amit Bahl, High-Speed PCB Design Guide, Sierra Circuits Inc., 2020.

[50] Tim Williams, EMC for Product Designers Fifth edition, Elsevier Ltd., 2017.

[51] https://hwbot.org/benchmark/cpu_frequency/rankings#start=0#interval=20.

[52] E. Sicard, J. F. Wu, R. J. Shen et al., Recent advances in electromagnetic compatibil-ity of 3D-ICs-part I, IEEE Electromagn. Compat. Mag., 4(4), 79–89, 2015.

[53] E. Sicard, Future needs in EMC of ICs: Are you hearing the voice of Industry, EMC Compo 2015, Edinburgh, 10-13th Nov, 2015.

[54] K. Patra, S. Dhar and B. Gupta, Radiation from simple and perturbed arbitrarily curved microstrip lines, Asia-Pacific Microwave Conference (APMC), pp. 1-4, 2016.

[55] Ming-Ju Tsai and N. G. Alexopoulos, Via hole modeling for an electromagnetically coupled patch antenna, Proceedings of IEEE Antennas and Propagation Society

International Symposium and URSI National Radio Science Meeting, pp. 1194-1197 vol.2, 1994.

[56] International technology roadmap for semiconductors, 2016, http://www.itrs.net.

[57] L. J. van der Pauw, The Radiation of Electromagnetic Power by Microstrip Configurations, in IEEE Transactions on Microwave Theory and Techniques, vol. 25, no. 9, pp. 719-725, Sep. 1977.

[58] C. A. Balanis, Antenna Theory: Analysis and Design, John Wiley and Sons, 1997.

[59] David K Cheng, Field and Wave Electromagnetics, Pearson Education Inc, Delhi, 2004.

[60] John D Kraus and Daniel A Fleisch, Electromagnetics with Applications, Mc Graw Hill Book Co,2005.

[61] Balanis C. A., Antenna Theory: Analysis and Design. Hoboken, New Jersey, USA: John Wiley & Sons; 2012.

[62] Kraus J. D., Antennas and Wave Propagation, Mc Graw-Hill, Inc, U.S.A.,2017.

[63] Er-Ping Li, Electrical Modeling and Design for 3D System Integration: 3D Integrated Circuits and Packaging, Signal Integrity, Power Integrity and EMC. Wiley-IEEE, April 2012.

[64] Larry Smith, Eric Bogatin: Principles of Power Integrity for PDN Design-Simplified: Robust and Cost Effective Design for High Speed Digital Products. Prentice Hall, April 2017.

[65] A. M. Sayegh and M. Z. Mohd Jenu, Prediction of radiated emissions from high-speed printed circuit board traces using dipole antenna and imbalance difference model, IET Sci. Meas. Technol., vol. 10, pp. 28–37, 2016.

[66] A. M. Sayegh and M. Z. Jenu, Closed-form expressions for estimating maximum radiated emissions from the traces of a Printed Circuit Board, Asia-Pacific Symposium on Electromagnetic Compatibility (APEMC)-2015, APEMC, 2015, pp. 620–623.

[67] A. M. Sayegh, M. Z. Mohd Jenu, S. Z. Sapuan and S. H. Dahlan, Analytical solution for maximum differential-mode radiated emissions of microstrip trace, IEEE Trans. Electromagn. Compat., vol. 58, pp. 1417-1424, 2016.

[68] B. W.-J. Wong and A. Cantoni, Modeling and analysis of radiated emissions and signal integrity of capacitively loaded printed circuit board interconnections, IEEE Trans. Electronmagn. Compat., vol. 54, pp. 1087–1096, 2012.

[69] G. Cerri, M. Mongiardo and T. Rozzi, Radiation from via-hole grounds in microstrip lines, IEEE MTT-S International Microwave Symposium Digest, pp. 341-344 vol.1,1994.

[70] N. Zhang, J. Kim, S. Ryu, and W. Nah, Prediction of common-mode radiated emission of PCB with an attached cable using imbalance difference model, IEICE Transaction on Communication, vol. E98-B, pp. 638–645, 2015.

[71] Mohd Zarar Mohd Jenu, Ahmed M. Sayegh, Syarfa Zahirah Sapuan, Maximum Radiated Emissions of Printed Circuit Board Using Analytical Methods, International Journal of Electrical and Computer Engineering (IJECE) Vol. 7, No. 6, December 2017, pp. 2919~2928.

[72] H. B. Bakoglu, Circuits, Interconnections, and Packaging for VLSI. Addison Wesley: Upper Saddle River, NJ, 1990..

[73] Yan Fu and Todd Hubing, Analysis of Radiated Emissions From a Printed Circuit Board Using Expert System Algorithms, IEEE Transactions on Electromagnetic Compatibility, vol. 49, no. 1, 2007.

[74] Graziano Cerri, Roberto De Leo, and Valter Mariani Primiani, Theoretical and Experimental Evaluation of the Electromagnetic Radiation From Apertures in Shielded Enclosures, IEEE Transactions on Electromagnetic Compatibility, vol 34, no. 4. November 1992.

[75] Buzincu, L, I; Anton, L; Deparateanu, D; Nicolaescu, M, Analysis of an Array of Rectangular Apertures Based on the Active Parameters of its Infinite Extension, 12th Intern. Conf. on Comm., Bucharest, 2018 ,WOS:000449526000040.

[76] C. Poschalkoand S. Selberherr, Calculation of the radiation from the slot of a slim enclosure with a cavity resonator model, Asia-Pacific Symposium on Electromagnetic Compatibility and 19th International Zurich Symposium on Electromagnetic Compatibility.

[77] Min Li, Joe Nuebel, James L. Drewniak, Richard E. DuBroff, Todd H. Hubing, and Thomas P. Van Doren, EMI from Cavity Modes of Shielding Enclosures—FDTD Modeling and Measurements, IEEE Transactions on Electromagnetic Compatibility, vol. 42, no. 1, 2000.